

1           **Increasing Notch signaling antagonizes PRC2-mediated silencing to promote**  
2                           **reprogramming of germ cells into neurons**

3  
4   Stefanie Seelk<sup>1\*</sup>, Irene Adrian-Kalchhauser<sup>2,3\*</sup>, Balázs Hargitai<sup>2</sup>, Martina Hajduskova<sup>1</sup>, Silvia  
5                           Gutnik<sup>2</sup>, Baris Tursun<sup>1†</sup> and Rafal Ciosk<sup>2†</sup>

6  
7   <sup>1</sup> Berlin Institute for Medical Systems Biology, Max-Delbrück-Center for Molecular  
8   Medicine, Robert-Rössle-Strasse 10, Berlin 13125, Germany

9   <sup>2</sup> Friedrich Miescher Institute for Biomedical Research, Maulbeerstr. 66, 4058 Basel,  
10   Switzerland

11   <sup>3</sup> Present address: Programm Mensch-Gesellschaft-Umwelt, Department of Environmental  
12   Sciences, University of Basel, Vesalgasse 1, 4051 Basel, Switzerland

13   \* These authors contributed equally to this work

14   † Correspondence: rafal.ciosk@fmi.ch; baris.tursun@mdc-berlin.de

15

16

17   Short Title: Notch antagonizes PRC2 for reprogramming

18   Keywords: Notch, GLP-1, PRC2, MES, UTX-1, stem cell, germline, reprogramming

19   **Abstract**

20   Cell-fate reprogramming is at the heart of development, yet very little is known about the  
21   molecular mechanisms promoting or inhibiting reprogramming in intact organisms. In the *C.*  
22   *elegans* germline, reprogramming germ cells into somatic cells requires chromatin perturbation.  
23   Here, we describe that such reprogramming is facilitated by GLP-1/Notch signaling pathway.  
24   This is surprising, since this pathway is best known for maintaining undifferentiated germline  
25   stem cells/progenitors. Through a combination of genetics, tissue-specific transcriptome  
26   analysis, and functional studies of candidate genes, we uncovered a possible explanation for  
27   this unexpected role of GLP-1/Notch. We propose that GLP-1/Notch promotes reprogramming  
28   by activating specific genes, silenced by the Polycomb repressive complex 2 (PRC2), and  
29   identify the conserved histone demethylase UTX-1 as a crucial GLP-1/Notch target  
30   facilitating reprogramming. These findings have wide implications, ranging from development  
31   to diseases associated with abnormal Notch signaling.

## 32    **Introduction**

33    Cell-fate decisions are controlled, on the one hand, by intercellular signaling and, on the other  
34    hand, by intrinsic mechanisms such as epigenetic chromatin modifications. The Notch  
35    signaling pathway is a highly conserved and widespread signaling mechanism (Artavanis-  
36    Tsakonas *et al.* 1999; Greenwald and Kovall 2013), which has been implicated in key cell-  
37    fate decisions such as the decision between proliferation and differentiation (Liu *et al.* 2010).  
38    Notch signaling has also been implicated in cellular reprogramming. Upon inhibition of Notch  
39    signaling, the oncogenic genes KLF4 and cMyc become dispensable for the generation of  
40    induced pluripotent stem cells (iPSCs) from mouse and human keratinocytes (Ichida *et al.*  
41    2014). In this setting, Notch inhibits reprogramming. Conversely, Notch signaling promotes  
42    transdifferentiation of pancreatic acinar cells to ductal cells (Sawey *et al.* 2007), or the  
43    conversion of hepatocytes into biliary cells in liver primary malignancy intrahepatic  
44    cholangiocarcinoma (ICC) (Sekiya and Suzuki 2012). Notch signaling can also affect  
45    reprogramming in normal development. In *C. elegans*, signaling through the GLP-1 and LIN-  
46    12 Notch receptors impedes reprogramming during embryogenesis and, during larval  
47    development, signaling through LIN-12 is required for the conversion of a rectal epithelial  
48    cell into a motoneuron (Jarriault *et al.* 2008; Djabrayan *et al.* 2012).

49        The role of epigenetic regulators in cell-fate decisions has been studied mostly in  
50    pluripotent cells cultured outside of their normal tissue environment (Meshorer and Misteli  
51    2006; Spivakov and Fisher 2007; Lessard and Crabtree 2010; Orkin and Hochedlinger 2011).  
52    Therefore, epigenetic regulation of stem cell identity in intact tissues remains poorly  
53    understood. Additionally, the impact of external cues, for example signaling from a stem cell  
54    niche to the recipient cell's chromatin remains equally unresolved. By contrast, *C. elegans*  
55    has been used as a model to study reprogramming in an intact organism (Horner *et al.* 1998;  
56    Fukushige *et al.* 1998; Zhu *et al.* 1998; Fukushige and Krause 2005; Ciosk *et al.* 2006;  
57    Jarriault *et al.* 2008; Yuzyuk *et al.* 2009; Riddle *et al.* 2013). In this model, germ cells can be  
58    directly reprogrammed into neurons by depleting specific chromatin modifiers such as LIN-  
59    53 (Rbbp4/7) or components of PRC2, and by concomitant overexpression of the

60 transcription factor CHE-1, which induces glutamatergic neuronal fate in a process which we  
61 refer to as Germ cell Conversion (GeCo) (Tursun *et al.* 2011; Patel *et al.* 2012).

62 Here, we identify the Notch signaling pathway as a critical player in this  
63 reprogramming model. This was unanticipated, since signaling through the Notch receptor  
64 GLP-1 (henceforth GLP-1<sup>Notch</sup>) from the somatic gonadal niche is known to maintain  
65 germline stem cell/progenitor fate (Kimble and Crittenden 2007). To understand this novel,  
66 reprogramming-promoting role of GLP-1<sup>Notch</sup>, we combined genetics with tissue-specific  
67 expression profiling. We identified genes regulated by GLP-1<sup>Notch</sup>, including genes recently  
68 shown to maintain the germline stem/progenitor cells (Kershner *et al.* 2014). Additionally,  
69 and unexpectedly, we found that many genes activated by GLP-1<sup>Notch</sup> signaling were also  
70 repressed by the cell fate-stabilizing chromatin regulator PRC2. We show that GLP-1<sup>Notch</sup> and  
71 PRC2 have an antagonistic effect on germ cell-fate decisions and demonstrate co-regulation  
72 of their common target, *utx-1*. Importantly, UTX-1 is a histone demethylase known to erase  
73 the gene-silencing methylation of histone H3 dependent on PRC2 (Maures *et al.* 2011; Jin *et*  
74 *al.* 2011; Vandamme *et al.* 2012). Thus, we propose that the GLP-1<sup>Notch</sup>-dependent induction  
75 of UTX-1 facilitates reprogramming by alleviating PRC2-mediated repression of alternative  
76 cell fates.

77

78



## 79     **Results**

### 80     ***GLP-1<sup>Notch</sup> enhances conversion of germ cells into neuron-like cells***

81     Germ cells can be converted into neuronal cells in intact *C. elegans* upon overexpression of  
82     the neuronal transcription factor CHE-1, simply by depleting the chromatin modifier LIN-53  
83     (Tursun *et al.* 2011; Patel *et al.* 2012). This GeCo phenotype can be followed in living  
84     animals by monitoring a reporter GFP expressed from the *gcy-5* promoter, which otherwise is  
85     induced in glutamatergic ASE neurons (Altun-Gultekin *et al.* 2001). In contrast to the  
86     spontaneous teratomatous differentiation of meiotic germ cells, observed in the absence of  
87     specific RNA-binding proteins (Ciosk *et al.* 2006; Biedermann *et al.* 2009; Tocchini *et al.*  
88     2014), GeCo is preferentially observed in the pre-meiotic, proliferating germ cells (Tursun *et*  
89     *al.* 2011; Patel *et al.* 2012). Consistently, removing the proliferating germ cells, by inhibiting  
90     the GLP-1<sup>Notch</sup> signaling, prevents GeCo (Tursun *et al.* 2011). However, because the  
91     proliferating germ cells were eliminated, these experiments did not address a possible direct  
92     effect of GLP-1<sup>Notch</sup> signaling on GeCo. We began addressing this issue by examining the  
93     gonads of animals carrying the gain-of-function *glp-1* allele (*ar202*) (Pepper *et al.* 2003).  
94     These gonads are filled with proliferating germ cells and, upon depleting LIN-53 and  
95     overexpressing CHE-1, we observed that significantly more germ cells converted to ASE  
96     neurons (Figure 1A, Figure 1–source data 1). We refer to this enhanced GeCo as “GeCo+”.  
97     Detailed quantification revealed that the GeCo+ gonads contained more than twice the  
98     number of converted cells (Figure 1–figure supplement 1A, Figure 1–source data 1). The  
99     nuclei of these converted cells were reminiscent of neuronal nuclei and the cells displayed  
100     axo-dendritic projection (Figure 1–figure supplement 1B), as previously described (Tursun *et*  
101     *al.* 2011; Patel *et al.* 2012). To confirm that the GeCo enhancement depends on the canonical  
102     Notch signaling pathway, rather than an independent function of the GLP-1<sup>Notch</sup> receptor, we  
103     RNAi-depleted the transcriptional effector of GLP-1<sup>Notch</sup> signaling, *lag-1* (Christensen *et al.*  
104     1996). We exposed animals only after hatching to *lag-1* RNAi in order to avoid sterility,  
105     which is caused when animals are subjected to *lag-1* RNAi earlier (Supplemental file 1).  
106     RNAi-mediated knock-down of *lag-1* strongly inhibited GeCo (Figure 1B, Figure 1–source

107 data 1). Importantly, under these experimental conditions, we did not observe any obvious  
 108 reduction of germ cell numbers (Figure 1C, Figure 1–source data 1), suggesting a  
 109 proliferation-independent effect of GLP-1<sup>Notch</sup> signaling on cell-fate conversion. To  
 110 investigate this further, we tested GeCo efficiency on germ cells proliferating independently  
 111 of GLP-1<sup>Notch</sup> signaling. We took advantage of mutants in which, in the absence of two  
 112 meiosis/differentiation-promoting factors GLD-1 and GLD-2, germ cells proliferate  
 113 independently of GLP-1<sup>Notch</sup> (Kadyk and Kimble 1998). Specifically, we examined GeCo in  
 114 the loss-of-function *gld-1(q497) gld-2(q485)* mutants, which carried either wild-type *glp-1* or  
 115 the loss-of-function *glp-1(q175)* allele (Austin and Kimble 1987). Both mutant combinations  
 116 have previously been described to have tumorous germlines and impaired meiotic entry  
 117 (Kadyk and Kimble 1998; Hansen *et al.* 2004). In contrast to efficient GeCo observed in the  
 118 *gld-1(q497) gld-2(q485)* gonads, GeCo was strongly diminished in the *gld-1(q497) gld-*  
 119 *2(q485); glp-1(q175)* gonads, despite the ongoing germ cell proliferation (Figure 1D, Figure  
 120 1–source data 1). Counting the number of germ cells in these gonads revealed only a slight  
 121 difference (a 15% increase in the numbers in the double vs. triple mutant gonads), suggesting  
 122 that the strong enhancement of GeCo by GLP-1<sup>Notch</sup> signaling cannot be explained by  
 123 increased number of germ cells (Figure 1–figure supplement 2, Figure 1–source data 1). Since  
 124 it has been proposed that dividing cells have a higher propensity for cellular reprogramming  
 125 (Egli *et al.* 2008; Hanna *et al.* 2009), we also tested whether blocking the cell cycle would  
 126 affect the observed GeCo enhancement in *glp-1(gf)* gonads. As previously described (Fox *et*  
 127 *al.* 2011; Patel *et al.* 2012), we used hydroxyurea (HU) treatment to block the cell cycle in the  
 128 S phase. Blocking the cell cycle by HU did not diminish the GeCo<sup>+</sup> phenotype (Figure 1–  
 129 figure supplement 3, Figure 1–source data 1). Combined, these results suggest that GLP-1<sup>Notch</sup>  
 130 enhances GeCo independently from its role in promoting germ cell proliferation.

### 132 ***GLP-1<sup>Notch</sup> activates genes mainly on X chromosomes***

133 To understand the effects of GLP-1<sup>Notch</sup> on GeCo, we set out to identify genes regulated by  
 134 GLP-1<sup>Notch</sup> signaling in germ cells. To conduct analysis in morphologically similar tissue, we

again took advantage of the *gld-1 gld-2* double mutants that, combined with either loss-of-function or gain-of-function *glp-1* alleles, have morphologically similar gonads, filled with proliferating, undifferentiated germ cells (Figure 2–figure supplement 1) (Kadyk and Kimble 1998; Hansen *et al.* 2004). We combined *gld-1(q497) gld-2(q485)* mutations with either the temperature-sensitive loss-of-function (lf) *glp-1* allele (*e2144*), or the temperature-sensitive gain-of-function (gf) *glp-1* allele (*ar202*) (Priess *et al.* 1987; Pepper *et al.* 2003). Because GLD-1 and GLD-2 regulate gene expression at the posttranscriptional level only, we expected that transcriptionally regulated GLP-1<sup>Notch</sup> targets could be identified in this background.

To analyze gene expression, gonads were dissected from animals grown at the restrictive temperature in two independent experiments, and transcripts were analyzed with tiling arrays (GEO accession number GSE49395). We identified around 100 transcripts that were differentially expressed between the *gld-1 gld-2; glp-1(lf)* (Notch OFF) and *gld-1 gld-2; glp-1(gf)* (Notch ON) gonads (Figure 2A and Figure 2–figure supplement 2, Figure 2–source data 1). These changes were confirmed by quantitative RT-PCR (RT-qPCR) on selected transcripts (Figure 2–figure supplement2A, Figure 2–source data 1). Most differentially expressed transcripts were upregulated in the ‘Notch ON’ gonads, indicating a predominantly activating role of GLP-1<sup>Notch</sup> in germ cells. For simplicity, we will refer to the transcripts upregulated at least two fold in the ‘Notch ON’ gonads as ‘Notch-activated’. Some Notch-activated genes, such as *sel-8/Mastermind*, *lst-1*, and *epn-1/Epsin*, have been implicated in Notch signaling in other cell types (Doyle *et al.* 2000; Yoo 2004; Tian *et al.* 2004; Singh *et al.* 2011; Kershner *et al.* 2014).

To demonstrate that Notch-activated genes are functionally relevant for germ cell proliferation, we performed RNAi knockdown of Notch-activated genes (n=64) on animals carrying the gain-of-function *glp-1(ar202)* allele, and screened for enhancement or suppression of the tumorous gonad phenotype (Supplementary file 1; for detailed experimental procedure see Materials and Methods). Knocking down some of the Notch-activated genes (n=17, 26.6%) suppressed the tumorous phenotype, which agrees with predominantly proliferation-promoting role of GLP-1<sup>Notch</sup>. Interestingly, knocking down a

subset of the Notch-activated genes enhanced the tumor (n=8, 12.5%) (Supplementary file 1), suggesting that some of the Notch-activated genes may counteract proliferation. While some of these genes may function autonomously in the germline, others could affect the germline indirectly from the soma. To test this, we RNAi-depleted selected candidates in the *rrf-1* (*pk1417*) mutant background, which is permissive for RNAi in the germline but deficient in RNAi in many (but not all) somatic tissues (Kumsta and Hansen 2012). While depleting most candidates in the *rrf-1* background had similar effects on the germline as in the wild type (suggesting germline-autonomous function), in some cases the effects were abolished, suggesting that these genes function in the soma (Figure 2-figure supplement 3, Figure 2–source data 1).

Strikingly, we noticed that Notch-activated genes were enriched on the X-chromosome, the *C. elegans* sex chromosome. 45% of the Notch-activated genes were X-linked, which is four-fold more than expected by chance ( $p = 2.99e^{-14}$ ; Figure 2A and Figure 2–figure supplement 2B, Figure 2–source data 1). When analyzing only genes with higher than baseline germline expression values, the disproportional X-linkage of Notch-activated genes was even more striking (fifteen times more than expected by chance ( $p = 2.19e^{-38}$ ; Figure 2A and Figure 2–figure supplement 2B, Figure 2–source data 1). In the *C. elegans* germline, X-linked genes are largely silenced by the *C. elegans* PRC2 (Fong *et al.* 2002). Thus, the X chromosome bias among Notch-activated genes suggested a possible antagonistic relationship between GLP-1<sup>Notch</sup> and PRC2.

#### ***GLP-1<sup>Notch</sup> and PRC2 have antagonistic functions in the germline***

The *C. elegans* PRC2 consists of MES-2, -3, and -6 (Bender *et al.* 2004) and levels of the corresponding transcripts were essentially not altered by GLP-1<sup>Notch</sup> signaling (*mes-2*: absolute fold change (fc) -1.3747; *mes-3*: fc 1.003; *mes-6*: fc 1.037). To test for a functional relationship between GLP-1<sup>Notch</sup> and PRC2, we examined genetic interactions between GLP-1<sup>Notch</sup> and PRC2 mutants. At 20 °C, both the temperature-sensitive gain-of-function *glp-1(ar202)* and the homozygous loss-of-function *mes-2(bn11)* mutants, derived from

heterozygous mothers providing maternal MES-2 (*mes-2* M+Z- mutants), were viable and produced gonads with nearly wild-type appearance. The double *mes-2* M+Z-; *glp-1(ar202)* mutants, however, displayed distal and proximal tumors at the same temperature (Figure 2B; 32/32 examined gonads). PRC2 and GLP-1<sup>Notch</sup> thus interact functionally, and they appear to do so in a germ cell autonomous manner (Figure 2-figure supplement 3, Figure 2–source data 1).

Given the striking enrichment of Notch-activated genes on the X chromosome, and the genetic interaction between PRC2 and GLP-1<sup>Notch</sup>, we speculated that GLP-1<sup>Notch</sup> and PRC2 act on similar genes. To determine whether Notch-activated genes are also PRC2-repressed, we first determined putative PRC2 targets by expression analyses on isolated wild-type, M+Z- *mes-2* or *mes-6* mutant gonads (GEO accession number GSE49395). Consistent with the joint function of MES-2 and MES-6 in the PRC2 complex, a very similar set of genes was upregulated upon the loss of either protein (Figure 2C; henceforth ‘PRC2-repressed’ genes; also see (Gaydos *et al.* 2012). Indeed, those PRC2-repressed genes overlapped strongly with Notch-activated genes, particularly those linked to the X chromosome. Nearly all of the X-linked Notch-activated genes were also derepressed upon the loss of PRC2 (Figure 2C). This is consistent with the observed genetic interaction and suggests that increased GLP-1<sup>Notch</sup> signaling can induce expression of specific PRC2-repressed genes. This activation of the PRC2-repressed genes is not due to a global loss of the repressive tri-methylation of Histone H3 at lysine residue 27 (H3K27me3), since, upon examining gonads of different GLP-1<sup>Notch</sup> mutants, we observed no global loss of H3K27me3 in the germ cells (Figure 2–figure supplement 4).

#### ***GLP-1<sup>Notch</sup> signaling enhances reprogramming***

Germ cell conversion to neurons can be triggered not only by LIN-53 depletion but also by the depletion of PRC2 (Patel *et al.* 2012). Potentially, the depletion of LIN-53 could facilitate reprogramming by inhibiting PRC2, since the depletion of LIN-53 results in a global loss of H3K27me3 in the germline (Patel *et al.* 2012). Considering the antagonistic relation between

219 GLP-1<sup>Notch</sup> and PRC2 on cell proliferation and gene regulation, we wondered whether GeCo  
220 triggered by the depletion of PRC2 would be sensitive to Notch signaling. Indeed, GeCo was  
221 strongly enhanced in PRC2-depleted (*mes-2*, *mes-3* or *mes-6* RNAi) animals, when they also  
222 carried the gain-of-function *glp-1(ar202)* allele (Figure 3A, Figure 3–source data 1).  
223 Moreover, similar to the LIN-53–depleted *gld-1(q497) gld-2(q485); glp-1(q175)* gonads  
224 (Figure 1D), the loss of GLP-1 effectively prevented GeCo in PRC2–depleted *gld-1(q497)*  
225 *gld-2(q485); glp-1(q175)* gonads (Figure 3B, Figure 3–source data 1). Together, these results  
226 suggest that GLP-1<sup>Notch</sup> stimulates GeCo in PRC2-compromised gonads.

227

### 228 ***UTX-1 is required for GLP-1<sup>Notch</sup>-mediated GeCo enhancement***

229 To determine how GLP-1<sup>Notch</sup> might counteract PRC2, we depleted candidate Notch-activated  
230 genes (Supplementary file 1), and examined GeCo efficiency (Figure 4A, Figure 4–source  
231 data 1). The strongest suppression of the GeCo+ and GeCo phenotype was observed upon the  
232 depletion of *utx-1*, which also suppressed *mes-3* RNAi-mediated GeCo+ in *glp-1(ar202)*  
233 (Figure 4–figure supplement 1). Depletion of two other candidates, the uncharacterized  
234 C07G1.6 and the aldolase ortholog *aldo-1*, also suppressed GeCo+, albeit less efficiently  
235 (Figure 4A). Because UTX-1 was suggested to effect gonadal development by functioning in  
236 the somatic gonad (Vandamme *et al.* 2012), we re-examined GeCo efficiency upon *utx-1*  
237 RNAi in the *rrf-1(pk1417)* background. Importantly, in *rrf-1* mutants, RNAi is impaired in  
238 the somatic gonad, including the distal tip cell (DTC), which constitutes the germline stem  
239 cell niche (Kumsta and Hansen 2012). Because the suppression of GeCo+ upon *utx-1* RNAi  
240 was observed also in the *rrf-1* background, UTX-1 does not seem to enhance GeCo by  
241 functioning in the somatic gonad (Figure 4–figure supplement 1A).

242 Importantly, *utx-1* encodes a conserved H3K27me3 demethylase, an enzyme erasing  
243 the repressive mark deposited by PRC2 (Agger *et al.* 2007; Jin *et al.* 2011; Maures *et al.*  
244 2011), potentially explaining how its depletion impairs GeCo efficiency. However, a number  
245 of other H3K27me3 demethylases exist in *C. elegans* which prompted us to test whether  
246 depletion of these demethylases might have an effect on GeCo in the *glp-1(ar202)* gonads.

247 We RNAi-depleted *jmjd-1.2*, encoding a H3K9/27me2 demethylase (Kleine-Kohlbrecher *et al.* 2010), *jmjd-3.1*, *jmjd-3.2*, and *jmjd-3.3*, which were reported to demethylate H3K27me2/3  
248 (Agger *et al.* 2007; Kleine-Kohlbrecher *et al.* 2010; Zuryn *et al.* 2014), and, as a control,  
249 *jmjd-2*, encoding a H3K9/36 demethylase (Whetstine *et al.* 2006; Greer *et al.* 2014) (Figure  
250 4B, Figure 4—source data 1). Only the depletion of JMJD-1.2 suppressed GeCo<sup>+</sup> significantly,  
251 though to a lesser degree than the depletion of UTX-1 (Figure 4B, Figure 4—source data 1).  
252 The suppression of GeCo by the depletion of UTX-1 or JMJD-1.2 stresses the importance of  
253 counteracting PRC2 in reprogramming. However, only the expression of *utx-1* is activated by  
254 the GLP-1<sup>Notch</sup> signaling, suggesting that it is the activity of UTX-1, which is key for the  
255 reprogramming dependent on GLP-1<sup>Notch</sup> signaling.  
256

257

#### 258 ***GLP-1<sup>Notch</sup> and PRC2 regulate expression of the H3K27 demethylase UTX-1***

259 The inhibition of GeCo enhancement upon *utx-1* RNAi in the *rrf-1* background suggested that  
260 UTX-1 functions in the germline. To test the potential expression of *utx-1* in the germline, we  
261 constructed a strain expressing single copy-integrated, FLAG and GFP-tagged, functional  
262 UTX-1 (expressed from the endogenous *utx-1* promoter under the control of endogenous *utx-1*  
263 3'UTR). We found that this protein was indeed expressed in the germline (Figure 5—figure  
264 supplement 1). To examine the potential transcriptional regulation of *utx-1* expression by  
265 GLP-1<sup>Notch</sup> and PRC2, we also created a strain expressing GFP-tagged histone H2B from the  
266 *utx-1* promoter (*putx-1* reporter), under the control of an unregulated (*tbb-2*) 3'UTR. This  
267 construct was also single-copy integrated into a defined genomic location. With both the  
268 UTX-1 fusion protein and the *putx-1* reporter, we expected expression patterns similar to that  
269 of other reported GLP-1<sup>Notch</sup> target genes (Lamont *et al.* 2004; Lee *et al.* 2006; Kershner *et al.*  
270 2014). Among these, *lst-1* and *sygl-1* account for the role of GLP-1<sup>Notch</sup> in stem cell  
271 maintenance, and both genes are expressed in the distal-most stem cells/progenitors (Kershner  
272 *et al.* 2014). By contrast, both the UTX-1 fusion protein and the *putx-1* reporter were little or  
273 not expressed in the distal-most, proliferative part of the germline (Figure 5A-C; Figure 5—  
274 figure supplement 1). Concomitantly with progression through meiosis, their expression

increased toward the proximal end of the gonad (Figure 5A-C). When examining the existing mRNA hybridization patterns of Notch-activated and PRC2-repressed genes (33 genes), we noticed that half of these (18, all X-linked) are similarly expressed in the medial and/or proximal, but not the distal-most, gonads (Supplementary file 2), arguing against direct transcriptional activation of these genes by GLP-1<sup>Notch</sup> in the wild type. Nevertheless, in agreement with the expression analyses, we observed increased expression of the *putx-1* reporter in PRC2-depleted gonads; this increase occurred throughout the gonad, including the distal-most region (Figure 5A). *In situ* hybridization for the endogenous *utx-1* transcript also showed increased expression throughout the gonad in the absence of PRC2 (Figure 5-figure supplement 2). Moreover, expression of the *putx-1* reporter was higher upon increased GLP-1<sup>Notch</sup> activity in *glp-1(ar202)* mutants, including the distal-most region where, in the wild-type, *utx-1* is little or not expressed (Figure 5B). Importantly, we found that the activation of the *utx-1* promoter by Notch signaling was depended on the putative LAG-1/CSL binding sites within the promoter (Yoo *et al.* 2004), as deleting those sites reduced reporter expression by approximately one-fourth (Figure 5C). The interaction between LAG-1 and *utx-1* was also tested by chromatin immunoprecipitation (ChIP), performed on a strain expressing FLAG-tagged LAG-1 in either wild-type or *glp-1(ar202)* background (Figure 5D and Figure 5-figure supplement 3); the previously identified GLP-1<sup>Notch</sup> targets, *lst-1* and *sygl-1* (Kershner *et al.* 2014), served as positive controls for the ChIP. Expectedly, we observed the enhanced binding of LAG-1 to the *utx-1* promoter, indicating that *utx-1* is a transcriptional target of GLP-1<sup>Notch</sup> signaling. Summarizing, based on the observations in mutant backgrounds, PRC2 and GLP-1<sup>Notch</sup> signaling have antagonistic effects on *utx-1* transcription. However, in wild type, the endogenous levels of GLP-1<sup>Notch</sup> signaling are apparently insufficient to overcome PRC2-mediated repression of *utx-1* in the distal-most part of the gonad.

## Discussion

In the *C. elegans* germline, GLP-1<sup>Notch</sup> signaling is essential for maintaining a pool of undifferentiated stem cells/progenitors. Here, we report an unexpected role of GLP-1<sup>Notch</sup>



303 signaling in promoting cell fate reprogramming. To understand this phenomenon, we identified  
304 genes activated upon increased GLP-1<sup>Notch</sup> signaling. While the identified genes include the  
305 physiological GLP-1<sup>Notch</sup> targets, *sygl-1* and *lst-1*, many other genes, including *utx-1*, appear  
306 to be only weakly or not expressed in the distal-most region of the wild-type gonad, where  
307 both *sygl-1* and *lst-1* are induced by GLP-1<sup>Notch</sup> (Kershner *et al.* 2014). Thus, the wild-type  
308 levels of GLP-1<sup>Notch</sup> signaling are either insufficient to induce expression of many potential  
309 target genes (see below), or their expression is controlled by additional mechanisms, perhaps  
310 similarly to *lip-1* mRNA, which, while induced by GLP-1<sup>Notch</sup>, is post-transcriptionally  
311 degraded in the distal-most gonad (Lee *et al.* 2006). In addition to its major proliferation-  
312 promoting function, GLP-1<sup>Notch</sup> has been suggested to have a lesser role in promoting germ  
313 cell differentiation (Hansen *et al.* 2004). Some of the identified Notch-activated genes appear  
314 to promote germ cell differentiation, potentially explaining the proposed differentiation-  
315 promoting function of GLP-1<sup>Notch</sup>. However, whether these genes are activated by GLP-1<sup>Notch</sup>  
316 and promote differentiation under physiological conditions remains to be determined.

317       Many of the Notch-activated genes are repressed by PRC2, suggesting that the  
318 expression of these genes is determined by the crosstalk between the extrinsic intercellular  
319 signaling pathway, Notch, and the intrinsic chromatin modifier PRC2. Indeed, at least in the  
320 case of *utx-1*, PRC2 appears to prevent its inappropriate expression in the distal-most gonad,  
321 which, nevertheless, can be overcome upon increased GLP-1<sup>Notch</sup> signaling. Our findings  
322 suggest that GLP-1<sup>Notch</sup> antagonizes PRC2, at least in part, by stimulating expression of the  
323 H3K27 demethylase UTX-1, which is essential for the enhancement of cellular reprogramming.  
324 Previously, it was suggested that UTX-1 influences the germline by functioning in the  
325 somatic gonad (Vandamme *et al.* 2012.) However, by using the *rrf-1* background, which  
326 displays defective RNAi in the somatic gonad, including DTC (Kumsta and Hansen 2012),  
327 we found that the reprogramming-promoting role of UTX-1 is unlikely to depend on its  
328 function in the somatic gonad. Although we cannot fully exclude the possibility that the  
329 reprogramming-facilitating role of UTX-1 depends on its expression in another somatic tissue  
330 (such as the intestine, in which RNAi remains functional in the *rrf-1* mutant; Kumsta and

331 Hansen 2012), the germline expression of UTX-1 reported here suggests a germline-  
332 autonomous function. Consistent with this hypothesis, manipulating either PRC2 or GLP-  
333 1<sup>Notch</sup> affected the germline expression of *utx-1*.

334         Although additional factors, such as the uncharacterized C07G1.6 and the ortholog of  
335 the human Aldolase A (Kuwabara and O'Neil 2001; Shaye and Greenwald 2011) might  
336 contribute to reprogramming, they appear to be less critical. In addition to UTX-1, another  
337 H3K27/H3K9-demethylating enzyme, JMJD-1.2 (Kleine-Kohlbrecher *et al.* 2010), is required  
338 for enhanced reprogramming. Similar to UTX-1, JMJD-1.2 is likely to be directly involved in  
339 regulating chromatin accessibility, since its depletion results in increased levels of the  
340 repressive H3K9me2 and H3K27me2 modifications (Kleine-Kohlbrecher *et al.* 2010). The  
341 reprogramming-promoting role of JMJD-1.2 might indicate that, besides further demethylation  
342 of H3K27me2, perhaps also the removal of H3K9me2 facilitates GeCo. Future studies will  
343 shed light on this interesting question.

344         UTX-1 orthologs in other species contribute to tissue-specific chromatin signatures,  
345 for example during myogenesis or in cardiac development (Seenundun *et al.* 2010; Lee *et al.*  
346 2012), and have been implicated in germ cell and somatic reprogramming (Mansour *et al.*  
347 2012). Together with our data, these findings underscore the importance of UTX-1 in cellular  
348 reprogramming. Here, we suggest that one way the activity of UTX-1 may be stimulated to  
349 promote reprogramming is through its Notch signaling-dependent transcriptional activation.  
350 Interestingly, an antagonistic relationship between Notch and PRC2 has been also observed in  
351 T-cell leukemia (Ntziachristos *et al.* 2012). A fascinating possibility is that a regulatory  
352 principle described here could help explain the etiology of this and perhaps other human  
353 diseases linked to a pathological increase in Notch signaling.

354

## 355 MATERIALS AND METHODS

356

### 357 Nematode culture and mutants

358 Standard procedures were used to maintain animals. Worms (RRID:WB\_DL226) were grown  
359 at 25 °C unless stated otherwise. All heat-shock and temperature-sensitive strains were kept at  
360 15 °C. The *C. elegans* lines used in this study are listed and described in detail in the  
361 Supplementary file 3A.

362

### 363 RNA interference Experiments

364 The Enhancer-Suppressor screen on Notch targets was performed by feeding the animals with  
365 bacteria containing RNAi clones from the Ahringer and Vidal RNAi libraries. The clones not  
366 present in either of these libraries were cloned using primers as described in detail in the  
367 Supplementary file 3B. Experiments were performed at 15 °C, 20 °C or 25 °C using bleached  
368 embryos or overnight-synchronized L1 animals as stated in Supplementary file 1. The  
369 percentage of adult animals with the germline tumor phenotype was scored. To test germ cell  
370 autonomy, RNAi clones that induced significant suppression or enhancement in either setting  
371 were re-tested in a strain carrying the *glp-1(ar202)* (RRID:WB\_GC833) allele and,  
372 additionally the *rrf-1(pk1417)* (RRID:WB\_NL2098) mutation, which impairs RNAi primarily  
373 in the soma (Sijen *et al.* 2001). For this test, gravid adults were picked to RNAi plates and  
374 allowed to lay eggs over night at the semi-permissive temperature of 20 °C. Progeny was  
375 scored for enhancement or suppression of the germline tumorous phenotype at the young  
376 adult stage by DAPI staining of dissected gonads and scoring gonads as either wild type, as  
377 containing a proximal or distal tumor but still some eggs, or as completely tumorous.

378 Reprogramming experiments were carried out as F1-RNAi. Worms were put on RNAi plates  
379 and the following F1 generation was screened for phenotypes. Used RNAi clones are  
380 described in the Supplementary file 3B. The genotype of the worms used for germ cell  
381 reprogramming assays is BAT28 (*otIs305 ntlIs1*, RRID:WB\_OH9846, details in Supplemental  
382 Material an Methods). Animals were synchronized by bleaching and eggs were put on NGM-

383 agar containing *E.coli* OP50 (RRID:WB\_OP50) as food source to grow at 15 °C until worms  
384 reached the L4-stage. At this stage 15-20 worms were put per well of a 6-well plate,  
385 containing bacteria expressing dsRNA or carrying an empty RNAi vector, and grown at 15 °C  
386 until most of the F1 progeny reached the L3/L4 stage. The plates were heat-shocked at 37 °C  
387 for 30 min followed by an overnight incubation at 25 °C. Next day (~16 h post heat-shock)  
388 the plates were screened for progeny showing ectopic GFP induction in the germline. To  
389 induce the Glp-phenotype in *glp-1(ar202)*, the animals were shifted to room temperature 9 h  
390 before the heat-shock. For double RNAi, bacteria were grown as saturated culture. The OD<sub>600</sub>  
391 was measured to ensure that the bacteria were mixed in an appropriate 1:1 ratio and  
392 subsequently seeded on RNAi 6-well plates. The RNAi screen was performed as described  
393 above. The p-values were calculated using Student's *t*-test.

394

#### 395 **Cell cycle arrest by HU treatment and EdU staining**

396 Hydroxyurea (HU) treatment was carried out as previously described (Fox *et al.* 2011; Patel  
397 *et al.* 2012). HU was added to seeded RNAi-plates at a final concentration of 250 µM. L4  
398 worms (strain BAT32, details in Supplementary file 3A) grown on RNAi-plates were  
399 transferred to HU plates and incubated at room temperature for 5 h prior to heat-shock in  
400 order to induce CHE-1 expression. To test HU efficiency, control animals were treated with  
401 HU for 12 h with subsequent staining for DAPI and H3Ser10ph (pH3) antibody (Abcam  
402 #ab5176). After overnight incubation, the worms were assessed for GFP induction in the  
403 germline as described above. To assess the efficiency of the HU treatment, the *E. coli* strain  
404 of MG1693 (*E. coli* stock center), with incorporated 5-ethynyl-20-deoxyuridine (EdU), was  
405 used to feed L3/L4 worms. EdU in combination with DAPI staining was performed similar to  
406 the procedure described previously (Ito and McGhee 1987) and according to the  
407 manufacturers instructions (Invitrogen) of the EdU labeling kit. The Click-iT® EdU reaction  
408 buffer (Invitrogen) was mixed with Alexa Fluor® azide ('click' reaction) dye to detect cells  
409 that were replicating DNA. Staining was performed by freeze cracking worms after fixation  
410 with 2% formaldehyde.

411

412 ***C. elegans* tiling array analysis**

413 Parental animals were raised at 15 °C and shifted to 25 °C for egg laying. Offspring was  
414 dissected after the L4-adult transition. Fifty gonads per analyzed genotype in triplicates were  
415 dissected in M9 containing levamisole. RNA was isolated using the PicoPure RNA Isolation  
416 Kit (Applied Biosystems) according to the manufacturer's recommendations. Total RNA (200  
417 ng for the Notch ON/OFF experiments or 100 ng for the *mes*/wild-type experiments) was  
418 amplified using the Affymetrix GeneChip WT Amplified Double Stranded cDNA Synthesis  
419 Kit according to the manufacturer's instructions. The Affymetrix GeneChip WT Double-  
420 Stranded cDNA Terminal Labeling Kit was used for the fragmentation and labeling of 7.5 µg  
421 cDNA. The labeled material was loaded onto Affymetrix GeneChip *C. elegans* Tiling 1.0R  
422 Arrays and hybridized at 65°C for 16 h. The arrays were washed in an Affymetrix Fluidics  
423 station with the protocol FS450\_0001 and scanned in an Affymetrix GeneChip Scanner 3000  
424 with autoloader using Affymetrix GCC Scan Control v. 3.0.0.1214 software. All tiling arrays  
425 were processed in R (32,33) using Bioconductor (34) and the packages tilingArray and  
426 preprocessCore. The arrays were RMA background corrected and log2 transformed on the  
427 oligo level using the following command:

428 `expr <- log2 (rma.background.correct (exprs (readCel2eSet (filenames,rotated = TRUE))))).`

429 We mapped the oligos from the tiling array (bpmmap file from [www.affymetrix.com](http://www.affymetrix.com)) to the  
430 *C.elegans* genome assembly ce6 ([www.genome.ucsc.edu](http://www.genome.ucsc.edu)) using bowtie (Langmead *et al.*  
431 2009), allowing no error and unique mapping position. Expressions for individual transcripts  
432 were calculated by intersecting the genomic positions of the oligos with transcript annotation  
433 (WormBase WS190) and averaging the intensity of the respective oligos. For the *mes-4*/wt  
434 experiment, no quantile normalization was performed as the distributions for the *mes-4*  
435 mutant and the wt differed substantially. In the case of the Notch ON/OFF dataset quantile  
436 normalization was performed on the level of transcripts. The p-values were calculated in R  
437 with the hypergeometric distribution function "phyper".

438

439 **Validation of array analysis by RT-qPCR:**

440 RNA was isolated as described above. cDNA was synthesized with oligo dT primer using the  
441 ImProm II Reverse Transcription System from Promega according to the manufacturer's  
442 instructions. cDNA was used for qPCR with the Absolute QPCR SYBR Green ROX Mix  
443 (AbGene) on an ABI PRISM 7700 system (Applied Biosystems). qPCR reactions were  
444 performed as described previously (Biedermann *et al.* 2009). At least one primer in each pair  
445 is specific for an exon-exon junction. Sequences of the used primers are described in detail in  
446 the Supplementary file 3C. Mouse RNA was added before RNA isolation and reverse  
447 transcription, allowing for normalization to *cyt-c* and thereby correcting for variations in  
448 RNA isolation and reverse transcription. Standard curves for quantification were generated  
449 from a serial dilution of input cDNA for each primer pair. The amount of target present in  
450 each replicate was derived from the standard curve; an average was calculated for each of the  
451 triplicates. To compare total mRNA levels, the qPCR results were normalized to mouse *cyt-c*  
452 and to the *C. elegans* tubulin gene *tbb-2*, and fold enrichments were calculated.

453

454 ***In-situ* hybridization for *utx-1***

455 RNA *in situ* hybridization was performed and analyzed as previously described (Biedermann  
456 *et al.* 2009). Description of the primer pairs to generate probes from cDNA can be found in  
457 the Supplementary file 3C. Images were captured with a Zeiss AxioImager Z1 microscope,  
458 equipped with a Zeiss AxioCam MRc camera. Images were taken in linear mode of the  
459 Axiovision software (Zeiss) and processed with Adobe Photoshop CS4 in an identical  
460 manner.

461

462 **Chromatin Immunoprecipitation and qPCR (ChIP-qPCR)**

463 ChIP was performed as described (Askjaer *et al.* 2014). In brief, worms (strains OP591,  
464 RRID:WB\_OP591, and BAT890) were washed with M9 buffer and frozen as 'worm  
465 popcorn' in liquid nitrogen prior to pulverization with a mortar and pestle. The powder was  
466 dissolved in 10 volumes of 1,1 % formaldehyde in PBS + 1mM PMSF and incubated 10 min

467 with gentle rocking at room temperature with subsequent quenching for 5 min at room  
468 temperature by adding 2,5 molar glycine (final concentration 125 mM). After centrifugation  
469 with 4.000 g at 4 °C the pelleted was washed with ice-cold PBS+1mM PMSF and  
470 resuspended in 50 mM FA buffer (50 mM HEPES/KOH pH 7,5; 1mM EDTA; 1 % Triton-X  
471 100; 0,1% Sodium deoxycholate; 150 mM NaCl) + 1% sarkosyl + protease-inhibitors.  
472 Samples where sonicated twice using the Biorupter (15 times 30 sec ON, 30 sec OFF) on high  
473 settings at 4 °C followed by spinning at 13.000 g, 15 min, 4 °C. The supernatant  
474 corresponding to 4 mg of protein measured by Bradford assay was used for ChIPs. Samples  
475 were incubated with 50 µl of FLAG or HA antibodies coupled to µMACS<sup>TM</sup> microbeads  
476 (Milteny) (all blocked with 5% milk in FA-buffer). After incubating 1 h at 4 °C, the beads  
477 where washed in µMACS matrix columns in a magnetic rack with FA buffer containing 1M  
478 and 0.5 M NaCl and subsequent wash with TE and TEL buffer (0,25 M LiCl; 1 % Sodium  
479 deoxycholate; 1 mM EDTA; 10 mM Tris pH 8,0). Bound material was eluted with 65 °C pre-  
480 warmed 125 µl ChIP elution buffer (1% SDS, 250 mM NaCl, 10 mM Tris pH 8.0, 1 mM  
481 EDTA) and fixation was reversed using 2 µl of 10 mg/ml Proteinase K at at 50 °C for 1 h  
482 followed by 65 °C incubation overnight. DNA was purified using the Quiaquick PCR  
483 purification kit in a final volume of 40 µl and 1 µl was used for qPCR. Negative controls  
484 were used which were taken to assess the quality of the ChIP and fold enrichment of the  
485 target genes: lysates (N2 worms) which do not express the recombinant target protein with  
486 specific antibody (anti-FLAG coupled to µMACS beads) and lysates of worms expressing the  
487 recombinant target protein with unspecific antibody (anti-HA coupled to µMACS beads)  
488 controls, respectively. Primer for qPCRs were designed using Primer3Plus (Untergasser *et al.*  
489 2007) with the following settings: amplified region min. 100 bp - max. 200 bp; GC content:  
490 50-60 %; min. primer length: 18 nt - max. length 24 nt; melting temperature: min. 58 °C -  
491 max. 63 °C; max.; 3' self complementary allowance set to 1; max. allowed length of a  
492 mononucleotide repeat (max. poly-x): 3. Sequences of the used primers are listed in in the  
493 Supplementary file 3C. The qPCRs were run on CFX96 Touch<sup>TM</sup> Real-Time PCR Detection  
494 System from BioRad using the Maxima SYBR Green/ROX qPCR Master Mix (2X). The data

analysis was performed by calculating the  $\Delta\Delta C_t$ -values. Differences were assessed using Student's *t*-test.

#### **DAPI staining and counting of germ cells**

Worms were transferred to a slide and fixed by adding 10 - 20  $\mu$ l 95% ethanol and letting evaporate the ethanol. The ethanol fixation was repeated 2 more times before adding the DAPI solution in microscopy mounting media (vectashield from Vector or similar). The samples were sealed with a coverslip and nail polish before microscopy. Fluorescent micrographs were recorded with Zeiss AxioImager Z1 microscope and the SensicamII camera (PCO) and the micromanager software was used to capture Z-stack images with 0.5  $\mu$ m slice steps. Images subject to direct comparison were taken at identical exposure times. Counting of germ cells within the range from the DTC to the turn of gonadal arms of *glp-1(ar202); hsp::che-1; gcy-5::gfp* animals treated with either mock or *lin-53* RNAi was performed using the Z-stacks. Micromanager was used to control the Z-stack levels and the ImageJ plugin for cell counting for scoring the number of germ cells. Germ cell counts in gonads of Notch ON: *gld-2(q497) gld-1(q485) glp-1(ar202)* and Notch OFF: *gld-2(a497) gld-1(q485) glp-1(e2144)* (Figure 1–supplemental figure 2) and germline tumor phenotype in *glp-1(ar202)* and *glp-1(ar202); rrf-1(pk1417)* were scored after dissection, formaldehyde fixation and DAPI staining. For Notch ON and Notch OFF mutants, the central plane of the gonads was imaged and germ cells in the entire dissected gonad were counted using the CellCounter plugin with ImageJ. For each of the two strains, germ cells in the entire gonad of 15 dissected gonads were counted.

#### **Immunostaining and Antibodies**

Antibody staining of intact worms were performed using a freeze-crack procedure as described (Duerr 2006). In brief, after washing, worms were resuspended in 0.025% glutaraldehyde, and frozen between two frost-resistant glass slides on dry ice. Separating the glass slides while frozen creates additional cracks in the cuticle. Acetone/methanol or 4%



523 paraformaldehyde in 0.1M Phosphate buffer for 1 hour on ice fixation was used. Worms were  
 524 washed off the slides in PBS, blocked with 0.2% gelatin + 0.25% Triton in PBS, and stained.  
 525 Primary antibodies were diluted in PBS with 0.1% gelatin and 0.25% Triton and fixed worms  
 526 were incubated 4 h - overnight at 4 C. After PBS washes secondary antibody was applied for  
 527 3 h. After PBS washes worms were mounted with DAPI-containing mounting medium  
 528 (Dianova, #CR-38448) on glass slides. The primary antibodies used were anti-H3K27me3  
 529 (1:400; gift from Dr. Hiroshi Kimura); anti-HA (1:100, Roche #12CA5; acetone fixation);  
 530 anti-H3Ser10ph (1:400, Abcam, #ab14955; acetone fixation). Secondary antibodies were  
 531 Alexa Fluor dyes applied at 1:1000 dilution.  
 532 Stainings for H3K27me3 on dissected gonads were performed using anti-H3K27me3 from  
 533 Millipore (catalogue number 07-449, Lot 1959680; courtesy of Jan Padeken, Gasser  
 534 laboratory) on dissected gonads. Adult animals were dissected in M9 containing Levamisole,  
 535 fixed with 2% paraformaldehyde in PBS on poly-lysine coated slides, snap-frozen on dry ice,  
 536 freeze-cracked, incubated for 5 minutes in ice-cold DMF at -20°, washed for 5 min in PBS  
 537 0.1% Tween-20 at room temperature, blocked for 20 min in PBS 0.1% Tween-20 + 5% BSA  
 538 and incubated with the primary antibody over night at 4 °C. Secondary antibodies (Alexa 488,  
 539 goat anti rabbit, 1:500) were applied for 2h at room temperature. Slides were then washed  
 540 three times for 5 min in PBS 0.1% Tween-20 at room temperature and mounted with  
 541 Vectashield mounting medium containing DAPI.

542

### 543 **Transgenic animals and reporter GFP quantifications**

544 The transcriptional reporter gene *putx-1::gfp-h2b (rrrSi185)* was constructed from the 1302  
 545 bp putative promoter region of the gene *utx-1 (human UTX (Ubiquitously transcribed TPR on*  
 546 *X) homolog - 1)* fused to sequences encoding for GFP-H2B and the ubiquitously expressed  
 547 *tbb-2* 3'UTR using the Gateway Reporter Cloning System (Merritt *et al.* 2008). The reporter  
 548 gene *putx-1::gfp-h2b (rrrSi185 and rrrSi281)* was constructed with the following primers:

549 *putx-attB4*:

550 GGGGACAACTTTGTATAGAAAAGTTGGGATTTTATCTTCATCGGACCTG

551 putx-attB1 : GGGGACTGCTTTTTGTACAACTTGTGGCGGTGTGAGAAGCGATAC  
552 The full-length functional transgene *putx-1::flag-gfp-utx-1::utx-1 3'UTR (rrrSi189)* was  
553 constructed with the following primers: utx-1+3UTR+attB2 L  
554 ggggacagctttctgtacaaagtggACGACGAATCAGAACCTCTGCCGGAGGAGCGTCATgtaag  
555 utx-1+3UTR+attB3 R ggggacaactttgtataataaagtgaatgcggatactgccttctc  
556 The functional UTX-1 transgene *putx-1::flag-gfp-tev::utx-1::utx-1 3'utr(rrrSi189)* contains  
557 the same promoter as the transcriptional reporter, the full-length *utx-1* genomic sequence as  
558 well as the endogenous 3'UTR, and was equipped with N-terminal GFP, FLAG, and TEV  
559 tags. Transgenic animals were produced by single copy integration using the MosSCI direct  
560 insertion protocol (Frøkjaer-Jensen *et al.* 2008). The *rrrSi189* transgene is functional, as it  
561 rescues the *utx-1* mutant (*ok3553* allele). For GFP quantification, gonads were dissected from  
562 live animals in M9 buffer containing levamisole and mounted to glass microscopy slides  
563 (Frøkjaer-Jensen *et al.* 2008). Fluorescent micrographs were recorded with Zeiss AxioImager  
564 Z1 microscope and a Zeiss Axioncam MRm REV 2 CCD camera was used to capture images.  
565 Fluorescence intensities were quantified using ImageJ. GFP intensities were normalized to the  
566 picture background and corrected with the average autofluorescences measured in wild type  
567 (N2) gonads at the corresponding temperatures. Images subject to direct comparison were  
568 taken at identical exposure times and were processed with Adobe Photoshop CS4 in an  
569 identical manner. The numbers of analyzed gonads were as follows: n = 44 for wild-  
570 type reporter; n = 36 for *glp-1(gf<sup>ts</sup>)*; n = 55 for wild-type reporter on control RNAi; n  
571 = 48 for *mes-2(RNAi)*; n = 15 for *mes-3(RNAi)*; n = 29 for *mes-6(RNAi)*, and n = 20  
572 for LAG-1 binding sites deleted reporter.

573

#### 574 **Genetic interaction of *glp-1* and *mes-2***

575 Alleles used were *glp-1(ar202)* and *mes-2(bn11)*. Worms were grown at the semi-permissive  
576 temperature of 20 °C and gonads were dissected and DAPI-stained shortly after the L4-young  
577 adult transition.

578 The experiment was performed twice. In a first round, a low number of gonads was examined  
579 to identify whether the double mutant had a phenotype and to define phenotypic categories to  
580 score. Based on the observation of a clear and penetrant phenotype, gonads were scored in a  
581 second round according to the categories defined in the first round.

582

## 583 **ACKNOWLEDGMENTS**

584 We thank Sergej Herzog, Alina El-Khalili, Mei He, S. Muehlhaeusser and Iskra Katic for  
585 technical assistance, and the following FMI technology platforms: functional genomics,  
586 bioinformatics, advanced imaging and microscopy. We also thank the CGC, supported by the  
587 NIH, Tim Schedl and Dave Hansen for providing strains. We thank S. Gasser, J. Priess, D.  
588 Schübeler, G. Merdes and members of the Tursun and Ciosk groups for discussion and  
589 comments on the manuscript. This work was partly sponsored by the SBFI grant Nr.  
590 C15.0038 to RC. Friedrich Miescher Institute for Biomedical Research is sponsored by the  
591 Novartis Research Foundation. BT receives funding from ERC-StG-2014-637530 and ERC  
592 CIG PCIG12-GA-2012-333922 and is supported by the Max Delbrueck Center for Molecular  
593 Medicine in the Helmholtz Association.

594

595

## 596 **REFERENCES**

- 597 Agger K, Cloos PAC, Christensen J, Pasini D, Rose S, Rappsilber J, Issaeva I, Canaani E,  
598 Salcini AE, Helin K (2007) UTX and JMJD3 are histone H3K27 demethylases involved  
599 in HOX gene regulation and development. *Nature* **449**, 731–734.  
600 doi:10.1038/nature06145.
- 601 Altun-Gultekin Z, Andachi Y, Tsalik EL, Pilgrim D, Kohara Y, Hobert O (2001) A regulatory  
602 cascade of three homeobox genes, *ceh-10*, *ttx-3* and *ceh-23*, controls cell fate  
603 specification of a defined interneuron class in *C. elegans*. *Development (Cambridge,*  
604 *England)* **128**, 1951–1969.
- 605 Artavanis-Tsakonas S, Rand MD, Lake RJ (1999) Notch signaling: cell fate control and  
606 signal integration in development. *Science (New York, NY)* **284**, 770–776.
- 607 Askjaer P, Ercan S, Meister P (2014) Modern techniques for the analysis of chromatin and  
608 nuclear organization in *C. elegans*. *WormBook : the online review of C elegans biology*  
609 1–35. doi:10.1895/wormbook.1.169.1.

- 610 Austin J, Kimble J (1987) glp-1 is required in the germline for regulation of the decision  
611 between mitosis and meiosis in *C. elegans*. *Cell* **51**, 589–599.
- 612 Bender LB, Cao R, Zhang Y, Strome S (2004) The MES-2/MES-3/MES-6 Complex and  
613 Regulation of Histone H3 Methylation in *C. elegans*. *Current Biology* **14**, 1639–1643.  
614 doi:10.1016/j.cub.2004.08.062.
- 615 Biedermann B, Wright J, Senften M, Kalchhauser I, Sarathy G, Lee M-H, Ciosk R (2009)  
616 Translational repression of cyclin E prevents precocious mitosis and embryonic gene  
617 activation during *C. elegans* meiosis. *Developmental Cell* **17**, 355–364.  
618 doi:10.1016/j.devcel.2009.08.003.
- 619 Christensen S, Kodoyianni V, Bosenberg M, Friedman L, Kimble J (1996) lag-1, a gene  
620 required for lin-12 and glp-1 signaling in *Caenorhabditis elegans*, is homologous to  
621 human CBF1 and *Drosophila* Su(H). *Development (Cambridge, England)* **122**, 1373–  
622 1383.
- 623 Ciosk R, DePalma M, Priess J (2006) Translational regulators maintain totipotency in the  
624 *Caenorhabditis elegans* germline. *Science (New York, NY)* **311**, 851.
- 625 Djabrayan NJV, Dudley NR, Sommermann EM, Rothman JH (2012) Essential role for Notch  
626 signaling in restricting developmental plasticity. *Genes & Development* **26**, 2386–2391.  
627 doi:10.1101/gad.199588.112.
- 628 Doyle TG, Wen C, Greenwald I (2000) SEL-8, a nuclear protein required for LIN-12 and  
629 GLP-1 signaling in *Caenorhabditis elegans*. *Proceedings of the National Academy of  
630 Sciences of the United States of America* **97**, 7877–7881.
- 631 Duerr JS (2006) Immunohistochemistry. *WormBook : the online review of C elegans biology*  
632 1–61. doi:10.1895/wormbook.1.105.1.
- 633 Egli D, Birkhoff G, Eggan K (2008) Mediators of reprogramming: transcription factors and  
634 transitions through mitosis. *Nature Reviews Molecular Cell Biology* **9**, 505–516.  
635 doi:10.1038/nrm2439.
- 636 Fong Y, Bender L, Wang W, Strome S (2002) Regulation of the different chromatin states of  
637 autosomes and X chromosomes in the germline of *C. elegans*. *Science (New York, NY)*  
638 **296**, 2235–2238. doi:10.1126/science.1070790.
- 639 Fox PM, Vought VE, Hanazawa M, Lee M-H, Maine EM, Schedl T (2011) Cyclin E and  
640 CDK-2 regulate proliferative cell fate and cell cycle progression in the *C. elegans*  
641 germline. *Development (Cambridge, England)* **138**, 2223–2234.  
642 doi:10.1242/dev.059535.
- 643 Frøkjaer-Jensen C, Davis MW, Hopkins CE, Newman BJ, Thummel JM, Olesen S-P, Grunnet  
644 M, Jorgensen EM (2008) Single-copy insertion of transgenes in *Caenorhabditis elegans*.  
645 *Nature Genetics* **40**, 1375–1383. doi:10.1038/ng.248.
- 646 Fukushige T, Krause M (2005) The myogenic potency of HLH-1 reveals wide-spread  
647 developmental plasticity in early *C. elegans* embryos. *Development (Cambridge,  
648 England)* **132**, 1795–1805. doi:10.1242/dev.01774.
- 649 Fukushige T, Hawkins MG, McGhee JD (1998) The GATA-factor elt-2 is essential for  
650 formation of the *Caenorhabditis elegans* intestine. *Developmental Biology* **198**, 286–302.

651 Gaydos LJ, Rechtsteiner A, Egelhofer TA, Carroll CR, Strome S (2012) Antagonism between  
652 MES-4 and Polycomb Repressive Complex 2 Promotes Appropriate Gene Expression in  
653 C.&nbsp;elegans Germ Cells. *Cell Reports* **2**, 1169–1177.  
654 doi:10.1016/j.celrep.2012.09.019.

655 Greenwald I, Kovall R (2013) Notch signaling: genetics and structure. *WormBook : the online*  
656 *review of C elegans biology* 1–28. doi:10.1895/wormbook.1.10.2.

657 Greer EL, Beese-Sims SE, Brookes E, Spadafora R, Zhu Y, Rothbart SB, Aristizábal-Corrales  
658 D, Chen S, Badeaux AI, Jin Q, Wang W, Strahl BD, Colaiácovo MP, Shi Y (2014) A  
659 Histone Methylation Network Regulates Transgenerational Epigenetic Memory in  
660 C.&nbsp;elegans. *Cell Reports* **7**, 113–126. doi:10.1016/j.celrep.2014.02.044.

661 Hajnal A, Berset T (2002) The C.elegans MAPK phosphatase LIP-1 is required for the  
662 G(2)/M meiotic arrest of developing oocytes. *The EMBO Journal* **21**, 4317–4326.

663 Hanna J, Saha K, Pando B, Zon JV, Lengner CJ, Creighton MP, Oudenaarden AV, Jaenisch  
664 R (2009) Direct cell reprogramming is a stochastic process amenable to acceleration.  
665 *Nature* **462**, 595–601. doi:10.1038/nature08592.

666 Hansen D, Albert Hubbard EJ, Schedl T (2004) Multi-pathway control of the proliferation  
667 versus meiotic development decision in the Caenorhabditis elegans germline.  
668 *Developmental Biology* **268**, 342–357. doi:10.1016/j.ydbio.2003.12.023.

669 Hansen D, Wilson-Berry L, Dang T, Schedl T (2004) Control of the proliferation versus  
670 meiotic development decision in the C. elegans germline through regulation of GLD-1  
671 protein accumulation. *Development (Cambridge, England)* **131**, 93.

672 Horner MA, Quintin S, Domeier ME, Kimble J, Labouesse M, Mango SE (1998) pha-4, an  
673 HNF-3 homolog, specifies pharyngeal organ identity in Caenorhabditis elegans. *Genes &*  
674 *Development* **12**, 1947–1952.

675 Ichida JK, T C W J, Williams LA, Carter AC, Shi Y, Moura MT, Ziller M, Singh S, Amabile  
676 G, Bock C, Umezawa A, Rubin LL, Bradner JE, Akutsu H, Meissner A, Eggan K (2014)  
677 Notch inhibition allows oncogene-independent generation of iPS cells. *Nature chemical*  
678 *biology* **10**, 632–639. doi:10.1038/nchembio.1552.

679 Ito K, McGhee JD (1987) Parental DNA strands segregate randomly during embryonic  
680 development of Caenorhabditis elegans. *Cell* **49**, 329–336.

681 Jarriault S, Schwab Y, Greenwald I (2008) A Caenorhabditis elegans model for epithelial-  
682 neuronal transdifferentiation. *Proceedings of the National Academy of Sciences of the*  
683 *United States of America* **105**, 3790–3795. doi:10.1073/pnas.0712159105.

684 Jin C, Li J, Green CD, Yu X, Tang X, Han D, Xian B, Wang D, Huang X, Cao X, Yan Z,  
685 Hou L, Liu J, Shukeir N, Khaitovich P, Chen CD, Zhang H, Jenuwein T, Han J-DJ  
686 (2011) Histone demethylase UTX-1 regulates C. elegans life span by targeting the  
687 insulin/IGF-1 signaling pathway. *Cell metabolism* **14**, 161–172.  
688 doi:10.1016/j.cmet.2011.07.001.

689 Kadyk LC, Kimble J (1998) Genetic regulation of entry into meiosis in Caenorhabditis  
690 elegans. *Development (Cambridge, England)* **125**, 1803–1813.

691 Kershner AM, Shin H, Hansen TJ, Kimble J (2014) Discovery of two GLP-1/Notch target  
692 genes that account for the role of GLP-1/Notch signaling in stem cell maintenance. *PNAS*

693        **111**, 3739–3744. doi:10.1073/pnas.1401861111.

694        Kimble J, Crittenden S (2007) Controls of germline stem cells, entry into meiosis, and the  
695        sperm/oocyte decision in *Caenorhabditis elegans*. *Annual review of cell and*  
696        *developmental biology* **23**, 405.

697        Kleine-Kohlbrecher D, Christensen J, Vandamme J, Abarrategui I, Bak M, Tommerup N, Shi  
698        X, Gozani O, Rappsilber J, Salcini AE, Helin K (2010) A Functional Link between the  
699        Histone Demethylase PHF8 and the Transcription Factor ZNF711 in X-Linked Mental  
700        Retardation. *Molecular Cell* **38**, 165–178. doi:10.1016/j.molcel.2010.03.002.

701        Kumsta C, Hansen M (2012) *C. elegans* rrf-1 Mutations Maintain RNAi Efficiency in the  
702        Soma in Addition to the Germline. *PLoS ONE* **7**, e35428.  
703        doi:10.1371/journal.pone.0035428.s007.

704        Kuwabara PE, O'Neil N (2001) The use of functional genomics in *C. elegans* for studying  
705        human development and disease. *Journal of inherited metabolic disease* **24**, 127–138.

706        Lamont LB, Crittenden SL, Bernstein D, Wickens M, Kimble J (2004) FBF-1 and FBF-2  
707        regulate the size of the mitotic region in the *C. elegans* germline. *Developmental Cell* **7**,  
708        697–707. doi:10.1016/j.devcel.2004.09.013

709        Langmead B, Trapnell C, Pop M, Salzberg SL (2009) Ultrafast and memory-efficient  
710        alignment of short DNA sequences to the human genome. *Genome Biology* **10**, R25.  
711        doi:10.1186/gb-2009-10-3-r25.

712        Lee M-H, Hook B, Lamont LB, Wickens M, Kimble J (2006) LIP-1 phosphatase controls the  
713        extent of germline proliferation in *Caenorhabditis elegans*. *The EMBO Journal* **25**, 88–  
714        96. doi:10.1038/sj.emboj.7600901.

715        Lee S, Lee JW, Lee S-K (2012) UTX, a histone H3-lysine 27 demethylase, acts as a critical  
716        switch to activate the cardiac developmental program. *Developmental Cell* **22**, 25–37.  
717        doi:10.1016/j.devcel.2011.11.009.

718        Lessard JA, Crabtree GR (2010) Chromatin regulatory mechanisms in pluripotency. *Annual*  
719        *review of cell and developmental biology* **26**, 503–532. doi:10.1146/annurev-cellbio-  
720        051809-102012.

721        Liu J, Sato C, Cerletti M, Wagers A (2010) ‘Notch Signaling in the Regulation of Stem Cell  
722        Self-Renewal and Differentiation.’. (Elsevier Inc.) doi:10.1016/S0070-2153(10)91012-7.

723        Mansour AA, Gafni O, Weinberger L, Zviran A, Ayyash M, Rais Y, Krupalnik V, Zerbib M,  
724        Amann-Zalcenstein D, Maza I, Geula S, Viukov S, Holtzman L, Pribluda A, Canaani E,  
725        Horn-Saban S, Amit I, Novershtern N, Hanna JH (2012) The H3K27 demethylase Utx  
726        regulates somatic and germ cell epigenetic reprogramming. *Nature* **488**, 409–413.  
727        doi:10.1038/nature11272.

728        Maures TJ, Greer EL, Hauswirth AG, Brunet A (2011) The H3K27 demethylase UTX-1  
729        regulates *C. elegans* lifespan in a germline-independent, insulin-dependent manner.  
730        *Aging Cell* **10**, 980–990. doi:10.1111/j.1474-9726.2011.00738.x.

731        Merritt C, Rasoloson D, Ko D, Seydoux G (2008) 3' UTRs are the primary regulators of gene  
732        expression in the *C. elegans* germline. *Current biology : CB* **18**, 1476–1482.  
733        doi:10.1016/j.cub.2008.08.013.

734 Meshorer E, Misteli T (2006) Chromatin in pluripotent embryonic stem cells and  
735 differentiation. *Nature Reviews Molecular Cell Biology* **7**, 540–546.  
736 doi:10.1038/nrm1938.

737 Ntziachristos P, Tsigirgos A, Van Vlierberghe P, Nedjic J, Trimarchi T, Flaherty MS, Ferres-  
738 Marco D, da Ros V, Tang Z, Siegle J, Asp P, Hadler M, Rigo I, De Keersmaecker K,  
739 Patel J, Huynh T, Utro F, Poglio S, Samon JB, Paietta E, Racevskis J, Rowe JM,  
740 Rabadan R, Levine RL, Brown S, Pflumio F, Dominguez M, Ferrando A, Aifantis I  
741 (2012) Genetic inactivation of the polycomb repressive complex 2 in T cell acute  
742 lymphoblastic leukemia. *Nature Medicine* **18**, 298–303. doi:doi:10.1038/nm.2651.

743 Orkin SH, Hochedlinger K (2011) Chromatin connections to pluripotency and cellular  
744 reprogramming. *Cell* **145**, 835–850. doi:10.1016/j.cell.2011.05.019.

745 Patel T, Tursun B, Rahe DP, Hobert O (2012) Removal of Polycomb Repressive Complex 2  
746 Makes *C. elegans* Germ Cells Susceptible to Direct Conversion into Specific Somatic  
747 Cell Types. *Cell Reports*. doi:10.1016/j.celrep.2012.09.020.

748 Pepper AS-R, Killian DJ, Hubbard EJA (2003) Genetic analysis of *Caenorhabditis elegans*  
749 *glp-1* mutants suggests receptor interaction or competition. *Genetics* **163**, 115–132.

750 Priess J, Schnabel H, Schnabel R (1987) The *glp-1* locus and cellular interactions in early *C.*  
751 *elegans* embryos. *Cell* **51**, 601–611.

752 Riddle MR, Weintraub A, Nguyen KCQ, Hall DH, Rothman JH (2013) Transdifferentiation  
753 and remodeling of post-embryonic *C. elegans* cells by a single transcription factor.  
754 *Development (Cambridge, England)* **140**, 4844–4849. doi:10.1242/dev.103010.

755 Sawey ET, Johnson JA, Crawford HC (2007) Matrix metalloproteinase 7 controls pancreatic  
756 acinar cell transdifferentiation by activating the Notch signaling pathway. *Proceedings of*  
757 *the National Academy of Sciences of the United States of America* **104**, 19327–19332.  
758 doi:10.1073/pnas.0705953104.

759 Seenundun S, Rampalli S, Liu Q-C, Aziz A, Palii C, Hong S, Blais A, Brand M, Ge K,  
760 Dilworth FJ (2010) UTX mediates demethylation of H3K27me3 at muscle-specific genes  
761 during myogenesis. *The EMBO Journal* **29**, 1401–1411. doi:10.1038/emboj.2010.37.

762 Sekiya S, Suzuki A (2012) Intrahepatic cholangiocarcinoma can arise from Notch-mediated  
763 conversion of hepatocytes. *The Journal of clinical investigation* **122**, 3914–3918.  
764 doi:10.1172/JCI63065.

765 Shaye DD, Greenwald I (2011) OrthoList: a compendium of *C. elegans* genes with human  
766 orthologs. *PLoS ONE* **6**, e20085. doi:10.1371/journal.pone.0020085.

767 Sijen T, Fleenor J, Simmer F, Thijssen KL, Parrish S, Timmons L, Plasterk RH, Fire A  
768 (2001) On the role of RNA amplification in dsRNA-triggered gene silencing. *Cell* **107**,  
769 465–476.

770 Singh K, Chao MY, Somers GA, Komatsu H, Corkins ME, Larkins-Ford J, Tucey T, Dionne  
771 HM, Walsh MB, Beaumont EK, Hart DP, Lockery SR, Hart AC (2011) *C. elegans* Notch  
772 Signaling Regulates Adult Chemosensory Response and Larval Molting Quiescence.  
773 *Current Biology* **21**, 825–834. doi:10.1016/j.cub.2011.04.010.

774 Spivakov M, Fisher AG (2007) Epigenetic signatures of stem-cell identity. *Nature Reviews*  
775 *Genetics* **8**, 263–271. doi:10.1038/nrg2046.

776 Tian X, Hansen D, Schedl T, Skeath JB (2004) Epsin potentiates Notch pathway activity in  
777 *Drosophila* and *C. elegans*. *Development (Cambridge, England)* **131**, 5807–5815.  
778 doi:10.1242/dev.01459.

779 Tocchini C, Keusch JJ, Miller SB, Finger S, Gut H, Stadler MB, Ciosk R (2014) The TRIM-  
780 NHL Protein LIN-41 Controls the Onset of Developmental Plasticity in *Caenorhabditis*  
781 *elegans* (J Ahringer, Ed.). *PLoS genetics* **10**, e1004533.  
782 doi:10.1371/journal.pgen.1004533.

783 Tursun B, Patel T, Kratsios P, Hobert O (2011) Direct conversion of *C. elegans* germ cells  
784 into specific neuron types. *Science (New York, NY)* **331**, 304–308.  
785 doi:10.1126/science.1199082.

786 Untergasser A, Nijveen H, Rao X, Bisseling T, Geurts R, Leunissen JAM (2007)  
787 Primer3Plus, an enhanced web interface to Primer3. *Nucleic Acids Research* **35**, W71–4.  
788 doi:10.1093/nar/gkm306.

789 Vandamme J, Lettier G, Sidoli S, Di Schiavi E, Nørregaard Jensen O, Salcini AE (2012) The  
790 *C. elegans* H3K27 demethylase UTX-1 is essential for normal development, independent  
791 of its enzymatic activity. *PLoS genetics* **8**, e1002647. doi:10.1371/journal.pgen.1002647.

792 Whetstine JR, Nottke A, Lan F, Huarte M, Smolikov S, Chen Z, Spooner E, Li E, Zhang G,  
793 Colaiacovo M, Shi Y (2006) Reversal of Histone Lysine Trimethylation by the JMJD2  
794 Family of Histone Demethylases. *Cell* **125**, 467–481. doi:10.1016/j.cell.2006.03.028.

795 Yoo AS (2004) Crosstalk Between the EGFR and LIN-12/Notch Pathways in *C. elegans*  
796 Vulval Development. *Science (New York, NY)* **303**, 663–666.  
797 doi:10.1126/science.1091639.

798 Yuzyuk T, Fakhouri THI, Kiefer J, Mango SE (2009) The polycomb complex protein mes-  
799 2/E(z) promotes the transition from developmental plasticity to differentiation in *C.*  
800 *elegans* embryos. *Developmental Cell* **16**, 699–710. doi:10.1016/j.devcel.2009.03.008.

801 Zhu J, Fukushige T, McGhee JD, Rothman JH (1998) Reprogramming of early embryonic  
802 blastomeres into endodermal progenitors by a *Caenorhabditis elegans* GATA factor.  
803 *Genes & Development* **12**, 3809–3814.

804 Zuryn S, Ahier A, Portoso M, White ER, Morin MC, Margueron R, Jarriault S (2014)  
805 Sequential histone-modifying activities determine the robustness of transdifferentiation.  
806 *Science (New York, NY)* **345**, 826–829. doi:10.1126/science.1255885.

807



## 808 **FIGURE LEGENDS**

809

### 810 **Figure 1. GLP-1<sup>Notch</sup> signaling promotes reprogramming of germ cells.**

811 (A) GLP-1<sup>Notch</sup> enhances germ cell conversion (GeCo) into neuronal-like cells. Left:  
 812 fluorescent (top) and combined fluorescent/differential interference contrast (DIC)  
 813 micrographs (bottom) of adult animals. All animals ectopically expressed the pro-neuronal  
 814 transcription factor CHE-1 from a heat-shock promoter. *glp-1(ar202)* is a temperature-  
 815 sensitive gain-of-function allele of the Notch receptor. Animals were subjected to either mock  
 816 (control) or *lin-53* RNAi. Reprogrammed cells expressed a GFP reporter driven from the  
 817 neuronal *gcy-5* promoter (here an in other figures nGFP) and are outlined here and elsewhere  
 818 in yellow. Any signal outside the outlined region comes from somatic tissues. GeCo+  
 819 indicates animals that displayed a strongly enhanced GeCo phenotype. Scale bars = 10  $\mu$ m.  
 820 The cartoons depicting the GeCo and GeCo+ phenotypes are on the top right. The gonads are  
 821 shaded in grey and GFP-positive converted germ cells are green. Fractions of animals  
 822 displaying GeCo and GeCo+ are indicated below. At least 250 animals were quantified per  
 823 condition. P-values were calculated using Student's t-test:  $p^1 < 0,0001$ ;  $p^2 = 0,0006$ . Error bars  
 824 represent SEM. (B) The transcriptional effector of the GLP-1<sup>Notch</sup> signaling pathway, LAG-1,  
 825 is required for the GLP-1<sup>Notch</sup>-mediated enhancement of GeCo. Left: fluorescent micrographs  
 826 of adults expressing CHE-1-induced nGFP as explained above. GeCo is diminished upon the  
 827 depletion of LAG-1. White dashed lines outline the animal body. Scale bars = 10  $\mu$ m. Right:  
 828 the corresponding quantifications. At least 400 animals were quantified per condition. P-  
 829 values were calculated using Student's t-test:  $p^1 < 0,0001$ ;  $p^2 = 0,0018$ . Error bars represent  
 830 SEM. (C) GLP-1<sup>Notch</sup> signaling enhances GeCo independently from germ cell proliferation.  
 831 Shown are DAPI-stained gonads of *glp-1(ar202)* animals, expressing CHE-1-induced nGFP,  
 832 treated with either mock or *lin-53* RNAi. Germ cells were counted from the DTC (yellow  
 833 asterisk) to the turn of the gonad arm (dashed yellow line). 15 gonad arms per condition were  
 834 counted. Scale bars = 10  $\mu$ m. Quantifications are on the right. While greatly inhibiting GeCo,

835 *lag-1* RNAi did not change the number of germ cells. P-values were calculated using  
836 Student's t-test:  $p^1 = 0,89$ . Error bars represent SEM. (D) GLP-1<sup>Notch</sup> enhances GeCo  
837 independently from proliferation. Left: fluorescent micrographs of adults (with indicated  
838 genotypes), expressing CHE-1-induced nGFP. The first panel on the left shows a control,  
839 heterozygous (wild-type) *gld-1 gld-2/ ++*; *glp-1/ +* animal. The other panels show the  
840 homozygous *gld-1(q497)*, *gld-2(q485)* mutants, carrying either a loss-of-function (center) or a  
841 wild-type (right) allele of *glp-1*. Despite proliferating, germ cells in the *gld-1 gld-2*; *glp-1*  
842 gonads have lost the ability to undergo GeCo. Scale bars = 10  $\mu$ m. Right: the corresponding  
843 quantifications. At least 250 animals were quantified per condition. P-values were calculated  
844 using Student's t-test:  $p^1 = 0,0478$ ;  $p^2 = 0,0201$ . Error bars represent SEM.

845

846  
847 **Figure 2. GLP-1<sup>Notch</sup> and PRC2 regulate common targets and are functionally**  
848 **connected.**

849 (A) Notch-activated genes are biased for the sex chromosome linkage. Left: changes in  
850 transcript abundance in the 'Notch ON' versus 'OFF' dissected gonads (genotypes explained  
851 in Figure 2-supplemental figure 1A-B) were analyzed by microarrays. Transcripts upregulated  
852 at least 2-fold in the 'Notch ON' gonads are marked in red, those downregulated at least 2-  
853 fold in blue. Selected transcripts verified by RT-qPCR in Figure 2-supplemental figure 2A  
854 are additionally circled in black. Right: 5426 genes can be considered expressed in the gonad,  
855 based on the bimodal distribution of expression values. Only 3% of those expressed genes are  
856 X-linked. In contrast, nearly half (46%) of the expressed and Notch-activated transcripts are  
857 X-linked (see Figure 2-supplemental figure 2B for numbers). (B) GLP-1<sup>Notch</sup> and the  
858 Polycomb Repressive Complex 2 interact genetically. Left: DAPI-stained gonads from  
859 animals of the indicated genotypes. The *mes-2(bn11)* M+Z- single mutant gonads have wild-  
860 type appearance at 20 °C. The *glp-1(ar202)* gain-of-function mutants have an almost wild-  
861 type appearance at this temperature, except for an extended proliferative zone in the gonad,  
862 referred to as "distal tumor". At the same temperature, *mes-2(bn11)* M+Z-; *glp-1(ar202)*

double mutants developed extensive germline tumors in 32/32 of the examined gonads. The insets show close-ups from the indicated gonadal regions: the distal-most regions contain undifferentiated, proliferative germ cells in all mutants (a, c, e). However, while the single mutants contain oocytes with characteristically condensed chromosomes in the proximal gonads (b, d), the proximal gonads of the double mutants harbor proliferative germ cells (f). Scale bar = 30  $\mu$ m. Right: quantification of the phenotypes. “Distal tumor” indicates the presence of an elongated distal proliferative zone (approximately  $\frac{1}{2}$  of the distal gonad arm). “Extended” tumor indicates an extended distal tumor, few oocytes, and frequently also a proximal tumor. “Fully tumorous” indicates the absence of all differentiated cell types except for sperm produced during larval development. (C) GLP-1<sup>Notch</sup> and PRC2 target the same genes on the X chromosomes. The plots correlate changes in gene expression in M+Z- *mes-2* mutants with changes in gene expression changes in M+Z- *mes-6* mutants. Results are shown separately for X-linked (left) and autosomal (right) transcripts. Notch-activated genes (red in Figure 2A) are marked in red. Lightly shaded areas indicate transcripts that are at least 2-fold upregulated. The overlap between transcripts upregulated by GLP-1<sup>Notch</sup> and transcripts upregulated by the loss of CePRC2 is highly significant, particularly for the X-linked genes. The significance of the correlation was measured by hypergeometric distribution; X-linked Notch-activated vs. *mes-2* derepressed:  $p=1.31e-31$ ; X-linked Notch-activated vs. *mes-6* derepressed:  $p=7.41e-25$ ; autosomal Notch-activated vs. *mes-2* derepressed:  $p=1.47e-22$ ; autosomal Notch-activated vs. *mes-6* de-repressed:  $p=1.8e-12$ .

### Figure 3. GLP-1<sup>Notch</sup> enhances reprogramming upon the depletion of PRC2.

(A) Notch and PRC2 genetically interact in GeCo. Left: fluorescent micrographs of *glp-1(ar202)* gain-of-function mutants expressing CHE-1–induced neuronal GFP. The animals were subjected to control RNAi or RNAi against CePRC2 components (MES-2, 3, and 6), as indicated. Increased GLP-1<sup>Notch</sup> signaling enhanced the GeCo+ phenotype upon PRC2 depletion. Control RNAi (mock) for each genetic background did not result in any GeCo

(images not shown – see quantification). Right: the corresponding quantifications. P-values were calculated using Student's t-test:  $p^1 = 0,0006$ ;  $p^2 < 0,0001$ ;  $p^3 = 0,0536$ ;  $p^4 = 0,0001$ ;  $p^5 = 0,4035$ ;  $p^6 = 0,0003$ . At least 200 animals were scored per condition. Error bars represent SEM. (B) GLP-1<sup>Notch</sup> is required for GeCo in PRC2-depleted animals independently from proliferation. Left: fluorescent micrographs of adults expressing CHE-1–induced nGFP, with the genotypes indicated above the panels. The animals were subjected to RNAi as indicated on the left. The first column shows heterozygous, the other two homozygous animals carrying the loss of function alleles *gld-1(q497)*, *gld-2(q485)* and, in the central panel, *glp-1(q175)*. The animals were subjected to control RNAi or RNAi against PRC2 components (MES-2, 3, and 6). In the absence of GLP-1<sup>Notch</sup>, depletion of PRC2 components did not induce GeCo. Scale bars = 10  $\mu$ m. Right: the corresponding quantifications. P-values were calculated using Student's t-test:  $p^1 < 0,0456$ ;  $p^2 = 0,0337$ ;  $p^3 = 0,0070$ ;  $p^4 = 0,0637$ ;  $p^5 = 0,0080$ ;  $p^6 = 0,1259$ . At least 70 animals were scored per condition. Error bars represent SEM.

#### Figure 4. The H3K27 demethylase UTX-1 is required for GeCo enhancement

(A) UTX-1 is critical for GeCo enhancement. Candidate Notch-activated genes, selected from Supplementary file 2 with available RNAi clones, were assayed for a role in GeCo in *glp-1(ar202)* animals, expressing CHE-1–induced nGFP and treated with *lin-53* RNAi. While the additional depletion of *utx-1* had the strongest impact on GeCo<sup>+</sup> and GeCo, the depletion of C07G1.6 and *aldo-1* had a weaker effect. Representative fluorescence micrographs are below the quantification chart. White dashed line outline the animal body, yellow lines outline gonad areas with GeCo. P-values for GeCo<sup>+</sup> were calculated using Student's t-test:  $p^1 = 0,000013$ ;  $p^2 = 0,026$ ;  $p^3 = 0,021$ ;  $p^4 > 0,1$ . At least 250 animals were scored per condition. Error bars represent SEM. nGFP = *gcy-5::gfp*. Scale bars = 10  $\mu$ m. (B) As in A, but RNAi was performed against *jmjd-1.2* (H3K9/27me2 demethylase); *jmjd-3.1*, *jmjd-3.2*, and *jmjd-3.3*, (H3K27me2/3 demethylase); and *jmjd-2* (H3K9/36 demethylases). Only RNAi against *jmjd-1.2* suppresses GeCo<sup>+</sup>, though to a lesser degree compared to *utx-1* RNAi.

917 Representative fluorescence micrographs are below the quantification chart. P-values for  
918 GeCo+ were calculated using Student's t-test:  $p^1 = 0,0042$ ;  $p^2 = 0,035$ ;  $p^3 > 0,2$ . At least 190  
919 animals were scored per condition. Error bars represent SEM. Scale bars = 10 $\mu$ m.

920

921 **Figure 5. UTX-1 is regulated by GLP-1<sup>Notch</sup> and PRC2.**

922 (A - C) Expression of *utx-1* is regulated by PRC2 and GLP-1<sup>Notch</sup>. Top: dissected gonads  
923 expressing a GFP reporter, driven from the *utx-1* promoter (*putx-1::GFP*, fused to Histone 2B  
924 for nuclear localization to facilitate quantification), subjected to the indicated RNAi (A),  
925 crossed into the indicated genetic background (B) or carrying the indicated mutations in the  
926 reporter gene (C). a, b, and c indicate gonadal regions containing germ cells in mitosis (a),  
927 and leptotene/zygotene (b) or pachytene (c) stages of meiosis. Below: the corresponding GFP  
928 quantifications. The diagrams show GFP intensities relative to the control (indicated by green  
929 arrow) in regions a-c. Results are represented as average changes in the GFP intensity  
930 (relative to mock RNAi-ed or untreated animals). The error bars represent SEM. The numbers  
931 of analyzed gonads were as follows: n = 44 for wild-type reporter; n = 36 for *glp-1(ar202)*; n  
932 = 55 for wild-type reporter on control RNAi; n = 48 for *mes-2* (RNAi); n = 15 for *mes-3*  
933 (RNAi); n = 29 for *mes-6* (RNAi), and n = 20 for the LAG-1 binding sites deleted reporter.  
934 (A) The *putx-1::GFP* reporter is repressed by PRC2. In all *mes*-depleted gonads, the reporter  
935 was de-repressed in proliferating cells (a) as well as in more proximal gonadal regions (b-c).  
936 (B) The *putx-1::GFP* reporter is upregulated by GLP-1<sup>Notch</sup>. In the gain-of-function *glp-*  
937 *1(ar202)* mutant, the reporter was strongly derepressed in the proliferating cells in the distal-  
938 most gonad (a). Its expression was also increased in the more proximal regions (b-c), which,  
939 in this mutant background, contain proliferating cells instead of meiotic cells. (C) *putx-*  
940 *1::GFP* expression depends on the predicted LAG-1/CSL binding sites in the promoter. Upon  
941 deletion of putative LAG-1/CSL binding sites, the reporter expression was abolished. The  
942 changes in GFP intensities were highly significant (p-values were measured by independent t-  
943 tests)  $p^1=4.85^{-13}$ ,  $p^2=1.38^{-20}$ ,  $p^3=1.18^{-7}$ . (D) LAG-1 binds the *utx-1* promoter. Lysates of  
944 animals expressing FLAG-tagged LAG-1 (strain *wgIs591*; *lag-1::TY1::EGFP::3xFLAG*),

945 either in wild-type or *glp-1(ar202)* background, were subjected to ChIP-qPCR analysis of the  
946 indicated genes. Negative controls and additional tested genes are shown in Figure 5–  
947 supplemental figure 3. The qPCR amplicons were tested in at least three independent  
948 experiments. The results are shown as fold enrichment in anti-FLAG IP compared to IP with  
949 unspecific antibody. The 3'UTR of *lst-1* serves as a negative control. Interestingly, LAG-1  
950 binding in the *glp-1(ar202)* gain-of-function background is stronger to the *utx-1* promoter  
951 than to the reported GLP-1<sup>Notch</sup> targets *lst-1* and *sygl-1*. The asterisks indicate p-values < 0.05  
952 (Students *t*-test). Error bars represent SEM.

953

954

#### 955 SUPPLEMENTARY FIGURE LEGENDS

956

957 **Figure 1–figure supplement 1. *glp-1(gf)* gonads contain more than twice the number of**  
958 **converted cells which display neuronal characteristics.**

959 (A) For the quantification of *gcy-5::gfp*-positive cells per gonadal arm only the GeCo  
960 category of *wt* vs. *glp-1(gf)* was used because GeCo+ animals already show an extensive area  
961 of the gonad filled with *gcy-5::gfp*-positive cells with usually >100 cells/gonad making  
962 reliable counting impossible. Notably, animals with a seemingly similar extend of GeCo in *wt*  
963 vs. *glp-1(gf)* show a clear increase of *gcy-5::gfp*-positive cells per gonadal arm from approx.  
964 10 in *wt* to > 30 in *glp-1(gf)*. n(*wt*) = 75 gonadal arms, n(*glp-1(ar202)*) = 221 gonadal arms.  
965 The background of the loss of function allele *glp-1(q175)* leads to a significant decrease in  
966 GeCo as shown previously (Tursun *et al.* 2011). (B) A magnified view of *gcy-5::gfp*-positive  
967 (nGFP) cells, in a GeCo+ gonad from a *glp-1(gf)* animal. The converted cells show axo-  
968 dendritic projections (white arrow heads). The inset in the corresponding DIC image,  
969 magnified in the right-bottom corner, shows the nuclear morphology of a converted germ cell,  
970 which has lost the germ cell-specific ‘fried-egg’-like shape and instead shows nuclear  
971 speckles characteristic of a neuronal cell. Scale bar = 1  $\mu$ m.

972

973 **Figure 1–figure supplement 2. Germ cell numbers are similar between *gld-1 gld-2***  
974 **double and *gld-1 gld-2; glp-1* triple mutants.**

975 DAPI-stained gonads of *gld-1(q497) gld-2(q485)* or *gld-1(q497) gld-2(q485); glp-1(q175)*  
976 mutants, carrying the *hsp::che-1* and *gcy-5::gfp* transgenes. The gonads were imaged by  
977 fluorescent microscopy using Z-stack acquisitions. Germ cells from the DTCs (yellow  
978 asterisks) to the turn of the gonad arm (dashed lines) were counted. Below: 15 gonad arms per  
979 condition of L4 animals were counted. The numbers of germ cells differ only slightly (15%)  
980 in the double mutant vs. triple mutants background. Scale bars = 10  $\mu$ m. Error bars represent  
981 SEM.

982

983 **Figure 1–figure supplement 3. Blocking the cell cycle with Hydroxyurea does not inhibit**  
984 **GeCo+.**

985 (A) We used hydroxyurea (HU) treatment for 5 h to chemically block the cell cycle, which  
986 makes germ cells arrest in the S phase of the cell cycle. This arrest does not diminish the  
987 GeCo+ phenotype in *glp-1(gf)* gonads upon *lin-53* RNAi and *che-1(oe)*. At least 150 animals  
988 were quantified per condition. P-values were calculated using Student's t-test:  $p^1 = 0,1409$ ;  $p^2$   
989  $= 0,4583$ . Error bars represent SEM. The right panel shows examples of GeCo+ displaying  
990 animals based on *gcy-5::gfp* (nGFP) for HU-untreated (-HU) and HU-treated (+HU) animals.  
991 (B) The gonads were stained for EdU incorporation. Dashed lines outline gonads. Asterisks  
992 indicate distal tips of gonads. Scale bars = 10  $\mu$ m. (C) The gonads of *glp-1(ar202) gf*  
993 animals, which were treated with HU for 12 h and stained with DAPI and H3Ser10ph (pH3)  
994 antibody. The pH3-positive cells indicate condensed chromosomes of dividing cells. After 12  
995 h of HU treatment, the gonads contained, as expected, enlargement nuclei (arrowheads)  
996 (Gartner *et al.* 2004; Fox *et al.* 2011). The loss of pH3-positive cells indicates a cell cycle  
997 arrest. Asterisks indicate distal tips of gonads, dashed lines outline gonad. Scale bars = 10  
998  $\mu$ m.

999

**Figure 2—figure supplement 1. Examining transcriptional effects of GLP-1<sup>Notch</sup> signaling.**

(A) GLP-1<sup>Notch</sup> signaling counteracts the meiosis-promoting activity of several RNA binding proteins, of which GLD-1 and -2 are indicated. (B) Mutants that were used in this study: while the the loss-of-function (lf) alleles of *glp-1* cause the loss of germ cells, gain-of-function (gf) alleles result in a constitutive proliferation of germ cells. However, in the absence of the meiosis-promoting GLD-1 and GLD-2 proteins, germ cells continue to proliferate in the absence of GLP-1<sup>Notch</sup> activity. (C) Three representative gonads of Notch ON: *gld-2(q497) gld-1(q485); glp-1(ar202)* and Notch OFF: *gld-2(a497) gld-1(q485); glp-1(e2144)* animals are shown after dissection and DAPI staining. The central planes of the gonads were imaged. Nuclei were counted from those images using the CellCounter plugin with ImageJ. For each genetic background, germ cells in the entire gonad of 10 dissected gonads were counted. The quantification below revealed that the numbers of germ cells in both backgrounds are not changed. Error bars represent SD. Scale bar = 10  $\mu$ m.

**Figure 2—figure supplement 2. Analysis of Notch-activated genes.**

(A) Changes in the abundance of several transcripts (marked black in Fig. 2A) were verified independently from the genomic quantification by RT-qPCR. Colors correspond to fold-changes detected by microarrays (green), by RT-qPCR on genetically identical gonads (black), or by RT-qPCR on gonads with a different loss-of-function *glp-1* allele, *q175* (white).

\*This experiment was performed only once. The error bars represent SEM. (B) Although the number of genes on the arrays is almost equally distributed between the different chromosomes, the expression of X-linked genes is largely silenced in the germline. The table displays the numbers and fractions of genes on the different chromosomes, and the distributions of the Notch-activated genes. The cutoff between “not expressed” and “expressed” genes was set according to the bimodal distribution of expression values in the Notch ON and OFF arrays.



1027 **Figure 2-figure supplement 3. The PRC2 component MES-6 and most**  
1028 **enhancers/suppressors of *glp-1(ar202)* induced tumors appear to interact genetically**  
1029 **with GLP-1/Notch signaling in a germline-autonomous manner.**

1030 Each bar indicates the relative proportion of germlines with wild-type morphology (grey),  
1031 germlines that contain eggs but also a proximal or distal tumor (red), and germlines that are  
1032 fully tumorous (black). “n” indicates the number of DAPI-stained gonads scored for each  
1033 column. Empty vector 1 – 3 represent three independent replicates of the empty vector control  
1034 and demonstrate the robustness of the experiment. We observed that, for an unknown reason,  
1035 the *rrf-1(pk1417); glp-1(ar202)* double mutants were less likely to produce tumors at the  
1036 semi-permissive temperature of 20 °C. Nonetheless, the double mutant strain reacts to  
1037 enhancers, suppressors, and depletion of PRC2 components in a similar manner as the *glp-*  
1038 *1(ar202)* single mutant strain, with the exception of *mbk-1* and B0416.5 RNAi. Depletion of  
1039 *mes-2* and *mes-3* by RNAi was ineffective, since it did not enhance the tumorous phenotype  
1040 in either of the two strains.

1041

1042 **Figure 2-figure supplement 4. Global levels of H3K27me3 are unaffected by neither**  
1043 **loss-of-function nor gain-of-function mutations in *glp-1*.**

1044 Stainings of wild-type, gain-of-function *glp-1(ar202)*, Notch ON (*gld-2(q497) gld-1(q485);*  
1045 *glp-1(ar202)*) and Notch OFF (*gld-2(a497) gld-1(q485); glp-1(q175)*) gonads with antibodies  
1046 against H3K27me3 performed on whole worms (left panel, scale bars = 10 µm) or dissected  
1047 gonads (right panel, scale bars = 1 µm). The H3K27me3 levels do not differ globally between  
1048 the different mutant backgrounds. Asterisks indicate distal tips of gonads, dashed lines outline  
1049 gonad.

1050

1051

1052

**Figure 4—figure supplement 1. UTX-1 is required for the GeCo+ enhancement upon the depletion of PRC2**

(A) Adult *glp-1(ar202)* animals treated with *lin-53* or *mes-3* RNAi were additionally subjected to either control or *utx-1* RNAi. Depletion of *utx-1* strongly suppressed the GeCo+ phenotype. Suppression upon *utx-1* co-depletion with *lin-53* is also detectable in the *rrf-1(pk1417)* background which is permissive for RNAi in the germline but not in the somatic gonad and the DTC. Right: quantification: n = 715 were scored for *lin-53*; *utx-1* RNAi; n = 500 for *mes-3*; *utx-1* RNAi and n = 270 were scored for *lin-53*; *utx-1* RNAi in *rrf-1(pk1417)*. P-values were calculated using Student's t-test:  $p^1 = 0,0588$ ;  $p^2 = 0,0042$ ;  $p^3 = 0,2454$ ;  $p^4 = 0,01713$ ;  $p^5 = 0,40479$ ;  $p^6 = 0,00271$ . Error bars represent SEM. (B) anti-HA antibody staining for the 3xHA-tagged CHE-1 protein, which is being induced after heat-shock treatment in the different genetic backgrounds: *glp-1(ar202)*; *otIs305 (hsp<sup>prom</sup>::che-1::3xHA)* *ntIs1 (gcy-5<sup>prom</sup>::gfp)* treated with or without RNAi against *lin-53* and *utx-1*. As additional controls the strain *otIs305 (hsp<sup>prom</sup>::che-1::3xHA) ntIs1 (gcy-5<sup>prom</sup>::gfp)* with or without *lin-53* RNAi and heat shock treatment was used. No obvious changes in the induction of CHE-1::3xHA in the germlines of the different genetic backgrounds can be detected. Scale bars = 1  $\mu$ m.

**Figure 5—figure supplement 1. The functional *utx-1* transgene is expressed in the same pattern as a GFP reporter coupled to the *utx-1* promoter.**

Shown is an adult with an outlined gonad. The full-length GFP-tagged functional UTX-1 (*rrrSi189*) is repressed in the distal, proliferative part. Nuclei entering meiosis and developing oocytes express the fusion protein progressively stronger. This expression pattern is identical with the pattern seen in the *utx-1* promoter reporter strains (*rrrSi185*, *rrrSi281*).

1079 **Figure 5—figure supplement 2. The endogenous *utx-1* mRNA is upregulated in the**  
1080 **absence of the PRC2-component MES-6.**

1081 Shown are representative *in-situ* hybridisations against endogenous *utx-1* mRNA in dissected  
1082 gonads. In M+Z- *mes-6(bn66)* mutants, *utx-1* is upregulated throughout the gonads compared  
1083 to the control wild-type gonads. “AS” and “S” indicate antisense and sense probes.

1084

1085 **Figure 5—figure supplement 3. Testing LAG-1 binding to additional genes by ChIP.**

1086 Worm lysates (corresponding to 4 mg protein) of animals, with or without *lag-*  
1087 *1::TY1::EGFP::3xFLAG* (*wgIs59I*) transgene, were used for ChIP. Samples were incubated  
1088 with 50 µl of FLAG (‘specific’ FLAG antibody) or HA antibodies (‘unspecific’ HA antibody)  
1089 coupled to µMACS<sup>TM</sup> microbeads (Milty). As negative control, lysate N2 or *glp-1(ar202)*  
1090 worm lysates, which do not express the recombinant target protein, were used. Both negative  
1091 control lysates did not show any differences during the ChIP experiment when tested with  
1092 either specific antibody (anti-FLAG coupled to µMACS beads) or unspecific antibody (anti-  
1093 HA coupled to µMACS beads). Lysates of worms expressing the recombinant target protein  
1094 in N2 or *glp-1(ar202)* background were incubated with specific (anti-FLAG) and unspecific  
1095 (anti-HA) antibodies coupled to µMACS beads. The qPCR amplicons were tested in a  
1096 minimum of three independent ChIP-qPCR experiments. Quantification results are shown as  
1097 fold enrichment of anti-FLAG µMACS<sup>TM</sup> beads using *wgIs59I* lysate over anti-FLAG  
1098 µMACS<sup>TM</sup> beads using lysate without *wgIs59I* (*no lag-1::TY1::EGFP::3xFLAG*). Primer for  
1099 qPCRs (sequence details above) were designed using Primer3Plus (Untergasser *et al.* 2007).  
1100 The FLAG-beads using lysates with *lag-1::TY1::EGFP::3xFLAG* show specific enrichment  
1101 for tested target genes thereby validating the specificity of the ChIP. The asterisks indicates p-  
1102 values < 0.05 (Students *t*-test). Error bars represent SEM.

1103

1104

1105

1106

## 1107 SOURCE DATA LEGENDS

1108

1109 **Figure 1-source data 1.** Figure 1-source data 1A: Quantification of GeCo+ phenotype upon  
1110 RNAi against *lin-53* in *glp-1(ar202)* mutants. Figure 1-source data 1B: Quantification of  
1111 GeCo dependency on LAG-1. Figure 1-source data 1C: Quantification of germ cells in *glp-1*  
1112 (*ar202*) gonads with or without *lag-1* RNAi treatment. Figure 1-source data 1D:  
1113 Quantification of GeCo in different genetic backgrounds with highly proliferative germlines  
1114 upon RNAi against *lin-53*. Figure 1-figure supplement 1A source data: Quantification of gfp-  
1115 positive germ cells. Figure 1-figure supplement 2 source data: Quantification of germ cells in  
1116 different genetic backgrounds with highly proliferative germlines. Figure 1-figure  
1117 supplement 3A source data: Quantification of GeCo after cell cycle block with HU treatment.  
1118 More details can be found in the corresponding figure legends.

1119

1120 **Figure 2-source data 1.** Figure 2-source data 2A: Microarray results of differentially  
1121 expressed genes in Notch ON/OFF gonads. Figure 2-figure supplement 3 source data:  
1122 Quantification of germlines with wild-type morphology versus germlines with tumors upon  
1123 germline-autonomous RNAi against genetic interactors of PRC2. More details can be found  
1124 in the corresponding figure legends.

1125

1126 **Figure 3-source data 1.** Figure 3-source data 3A: Quantification of GeCo+ phenotype upon  
1127 RNAi against PRC2 subunits in *glp-1(ar202)* mutants. Figure 3-source data 3B:  
1128 Quantification of GeCo in different genetic backgrounds with highly proliferative germlines  
1129 upon RNAi against PRC2 subunits. More details can be found in the corresponding figure  
1130 legends.

1131

1132 **Figure 4-source data 1.** Figure 4-source data 4A: Quantification of GeCo+ upon RNAi  
1133 against *lin-53* and Notch-activated genes. Figure 4-source data 4B: Quantification of GeCo+  
1134 upon RNAi against *lin-53* and Histone demethylases. Figure 4-figure supplement 1A source

1135 data: Quantification of GeCo<sup>+</sup> upon RNAi against *lin-53* and *utx-1* with and without *rrf-1*  
1136 (*pk1417*) background. More details can be found in the corresponding figure legends.

1137

1138

#### 1139 **SUPPLEMENTARY FILES**

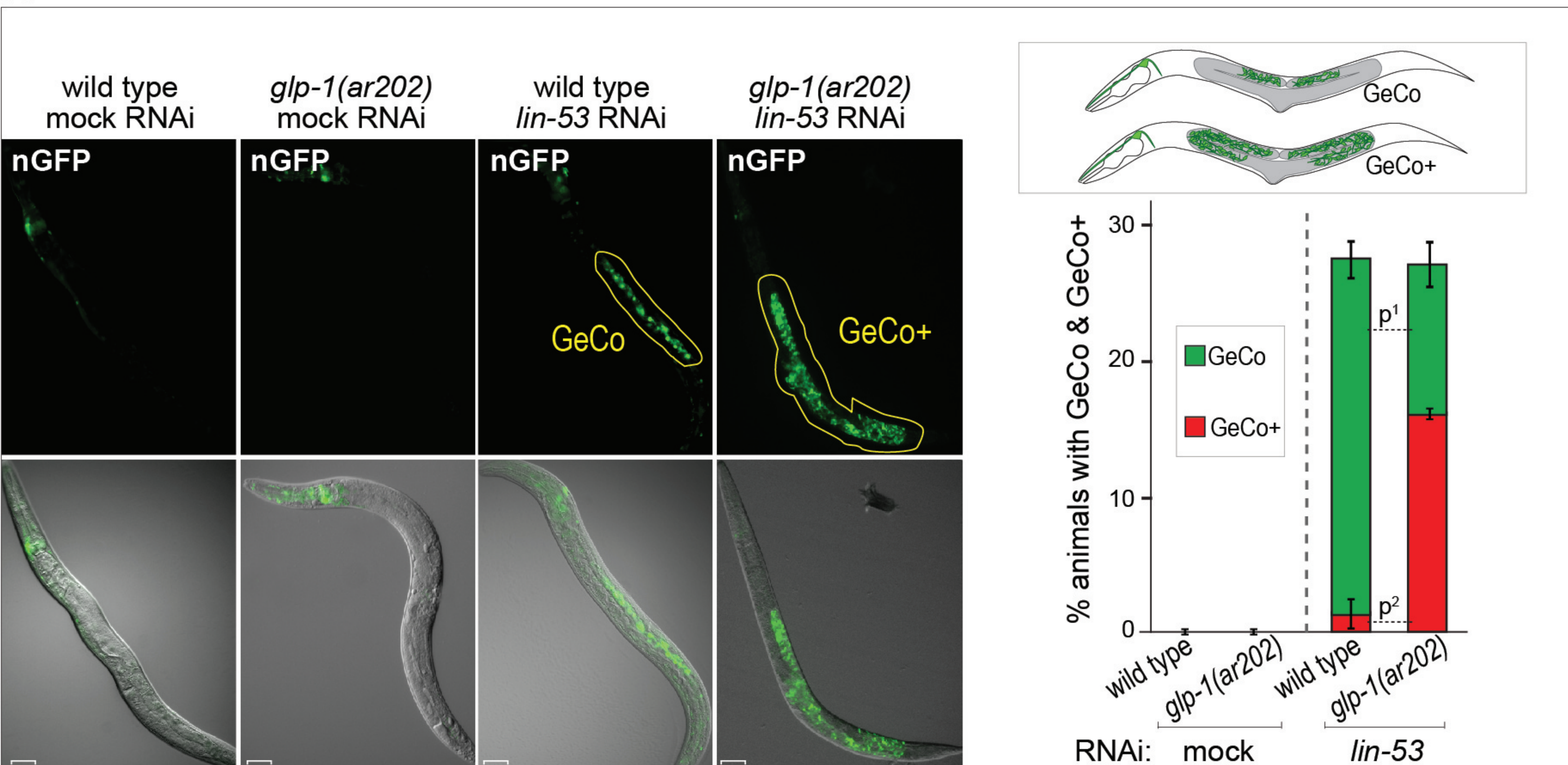
- 1140 - Supplementary file 1: Enhancement or suppression of tumorous phenotypes
- 1141 - Supplementary file 2: In situ hybridization patterns of Notch-activated genes
- 1142 - Supplementary file 3A: Information on used *C. elegans* strains used in the study
- 1143 - Supplementary file 3B: Information on RNAi clones used in this study
- 1144 - Supplementary file 3C: Information on primer design and sequences
- 1145 - Figure 1-source data 1: Contains Figure 1-source data 1A, Figure 1-source data 1B,  
1146 Figure 1-source data 1C, Figure 1-source data 1D, Figure 1–figure supplement 1A source  
1147 data, Figure 1–figure supplement 2 source data, Figure 1–figure supplement 3A source  
1148 data
- 1149 - Figure 2-source data 1: Contains Figure 2-source data 2A, Figure 2–figure supplement 3  
1150 source data
- 1151 - Figure 3-source data 1: Contains Figure 3-source data 3A, Figure 3-source data 3B
- 1152 - Figure 4-source data 1: Contains Figure 4-source data 4A, Figure 4-source data 4B,  
1153 Figure 4–figure supplement 1A source data

1154

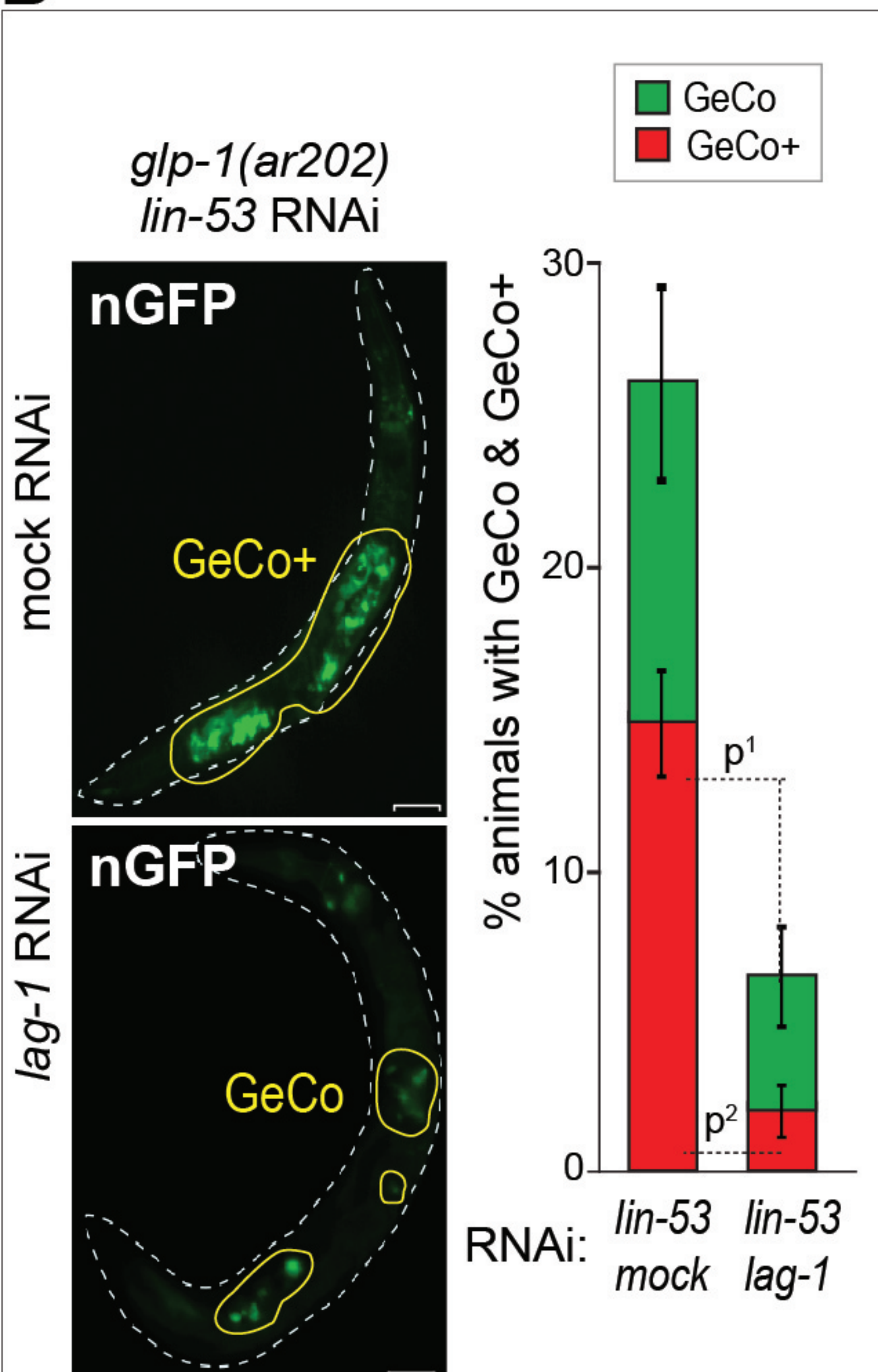
1155



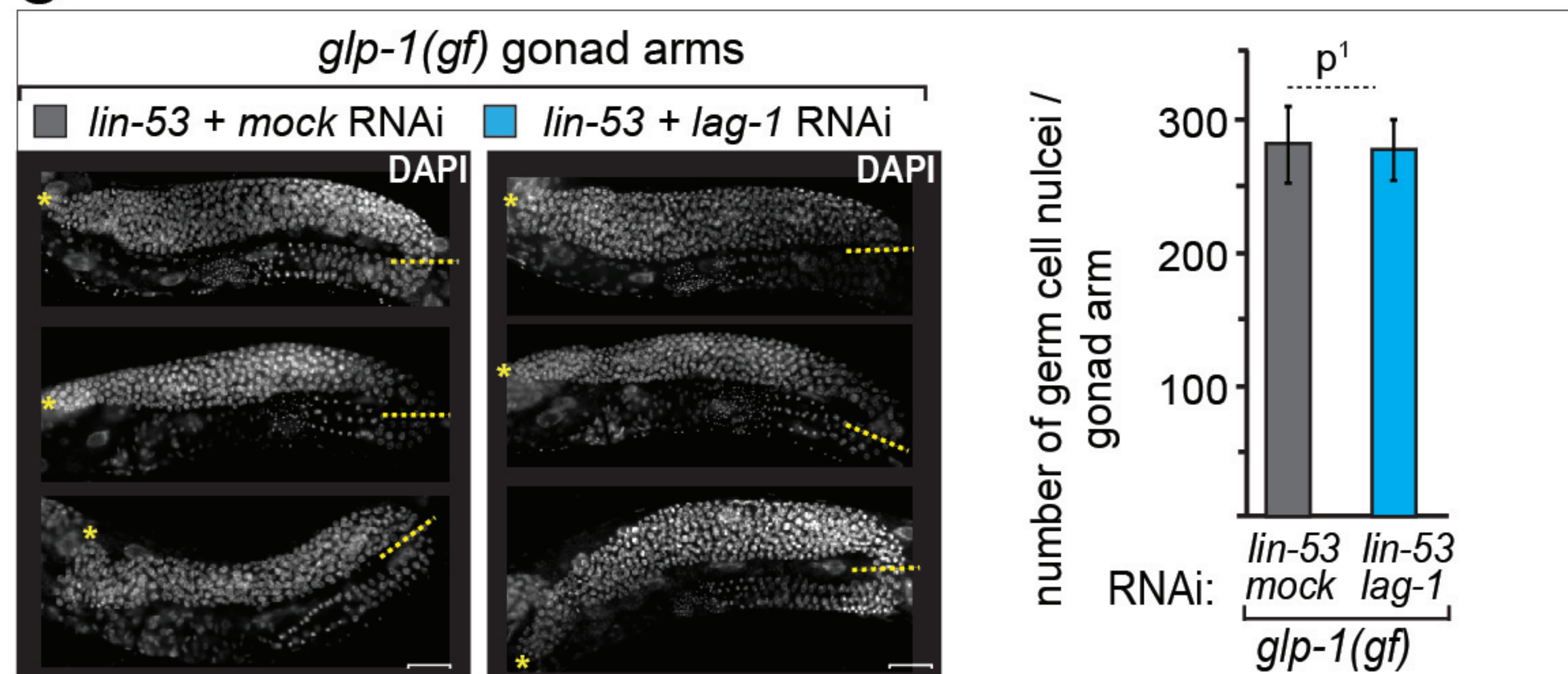
**A**



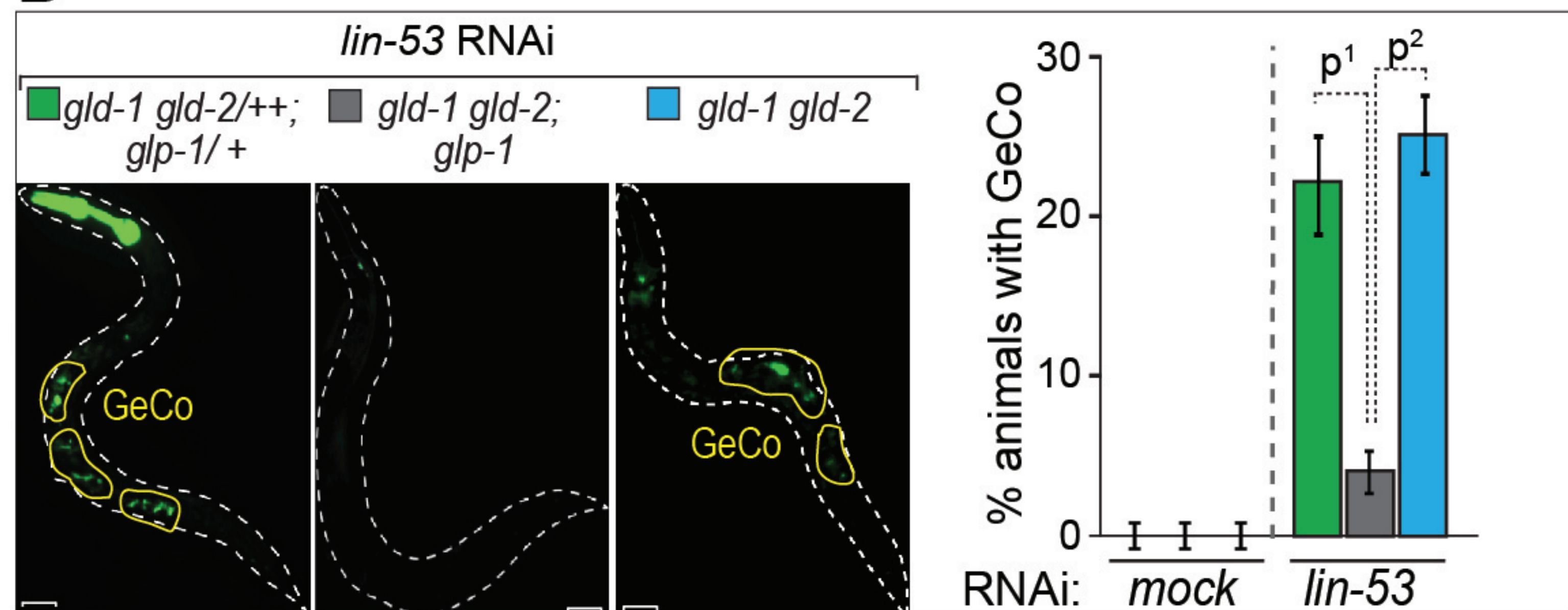
**B**



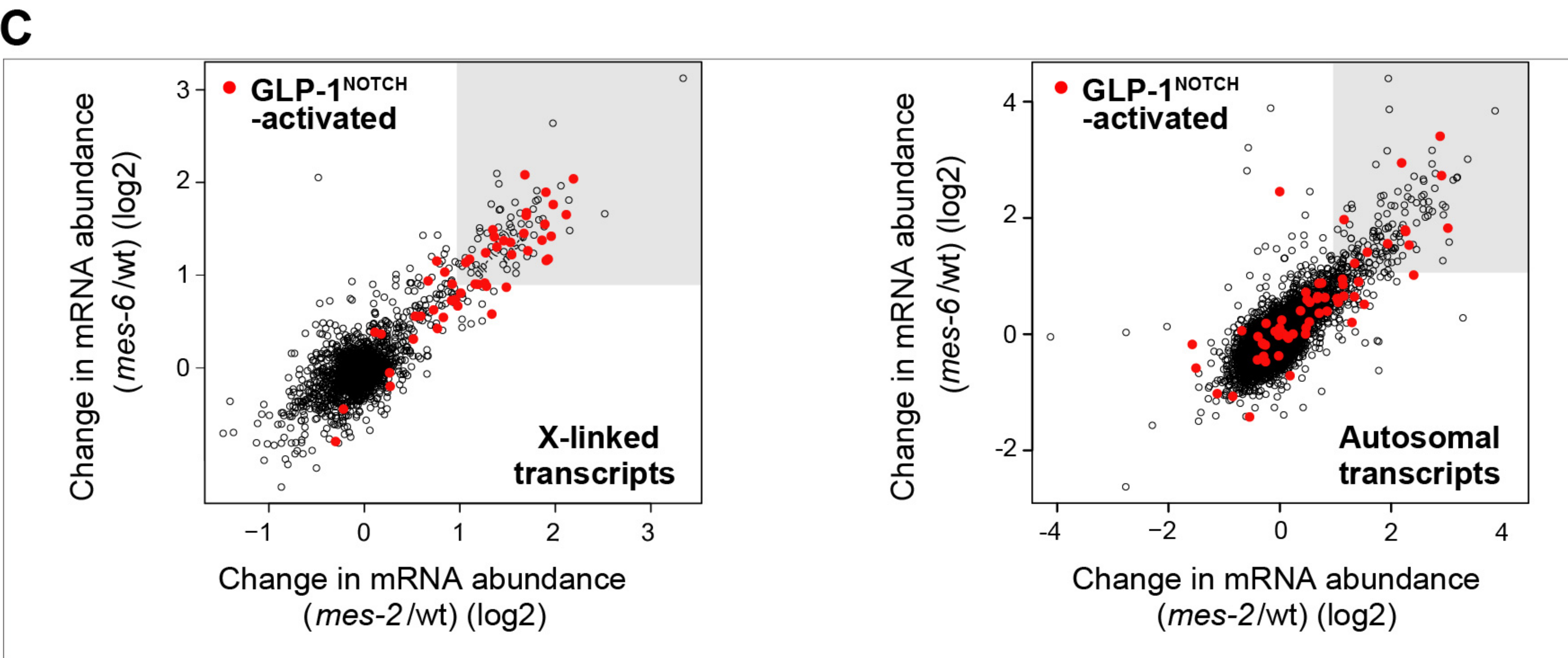
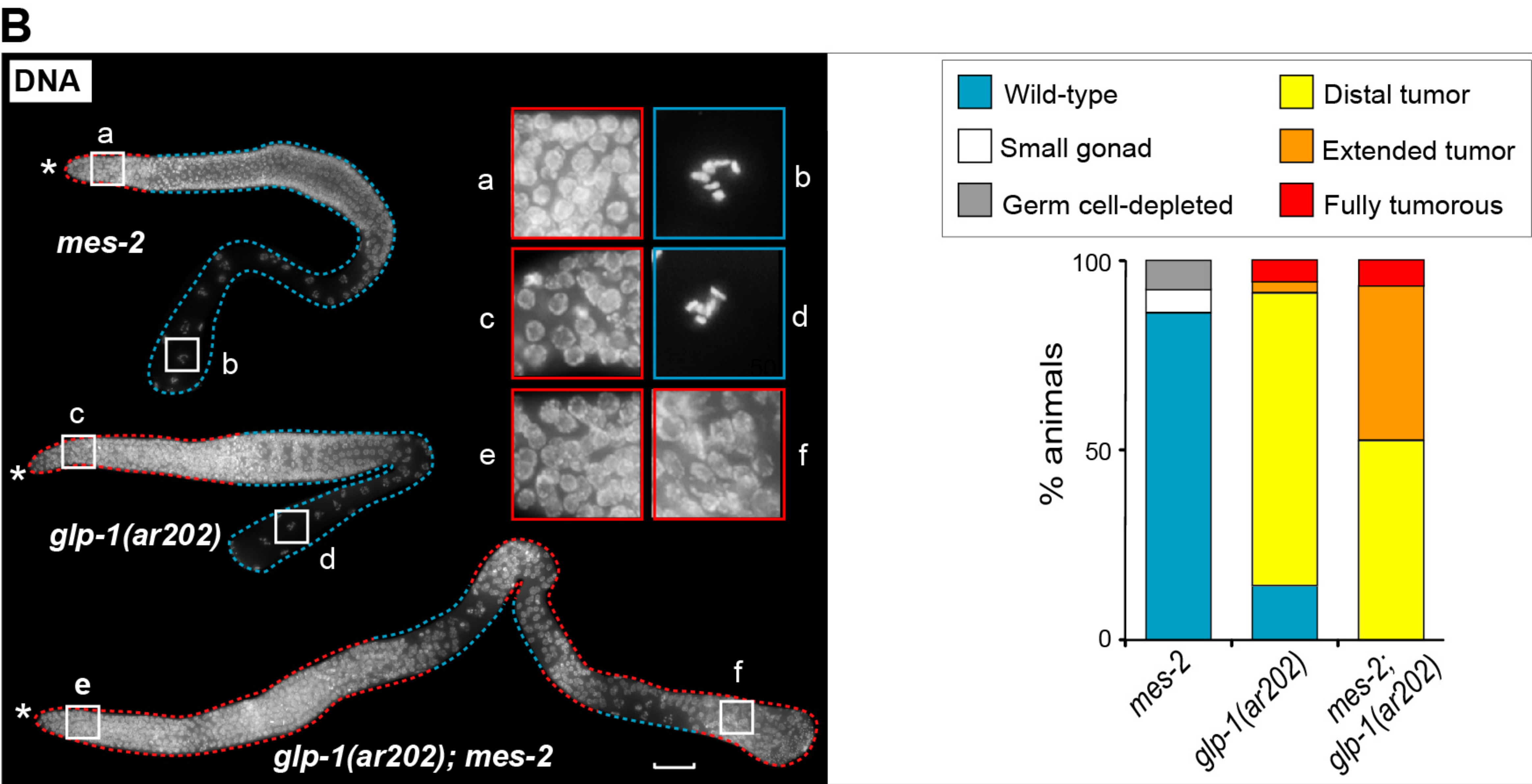
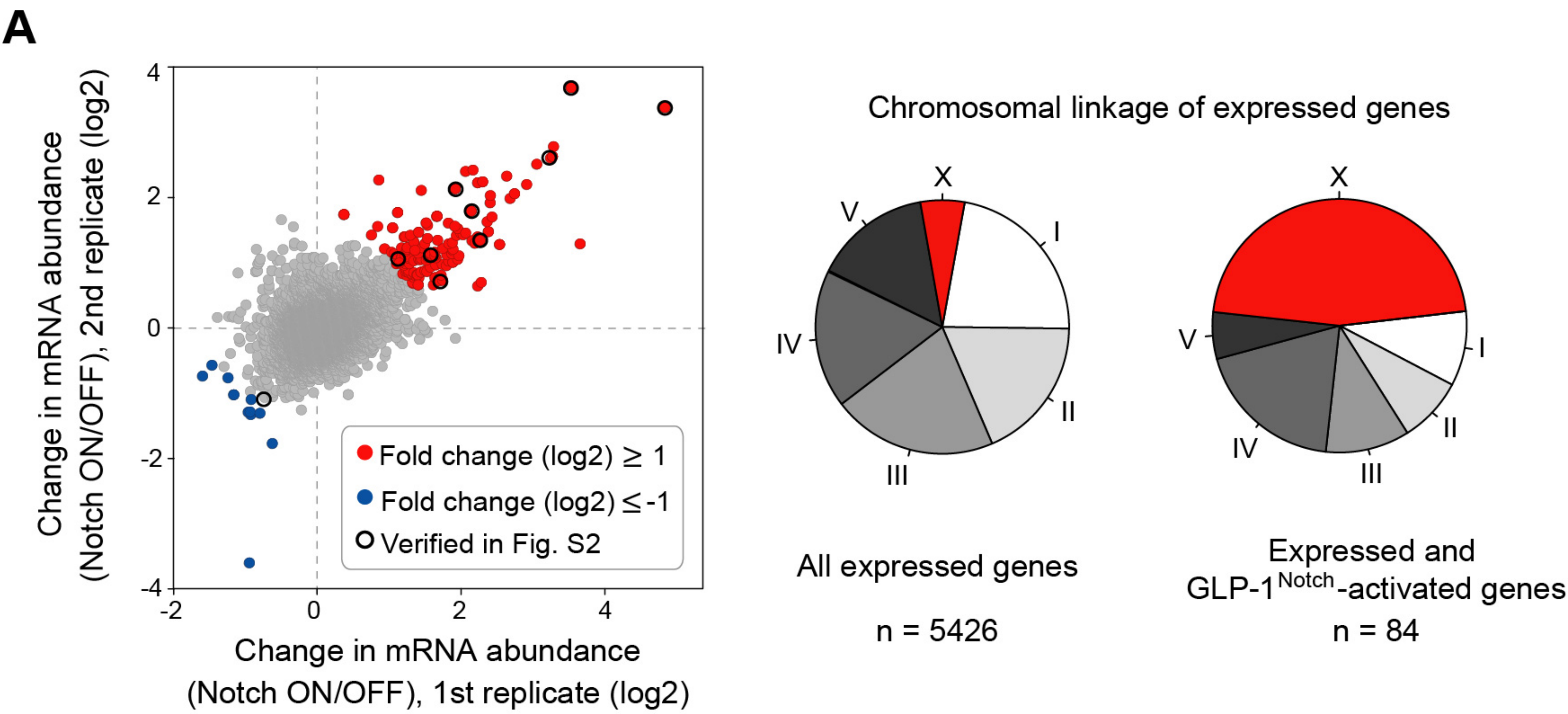
**C**



**D**





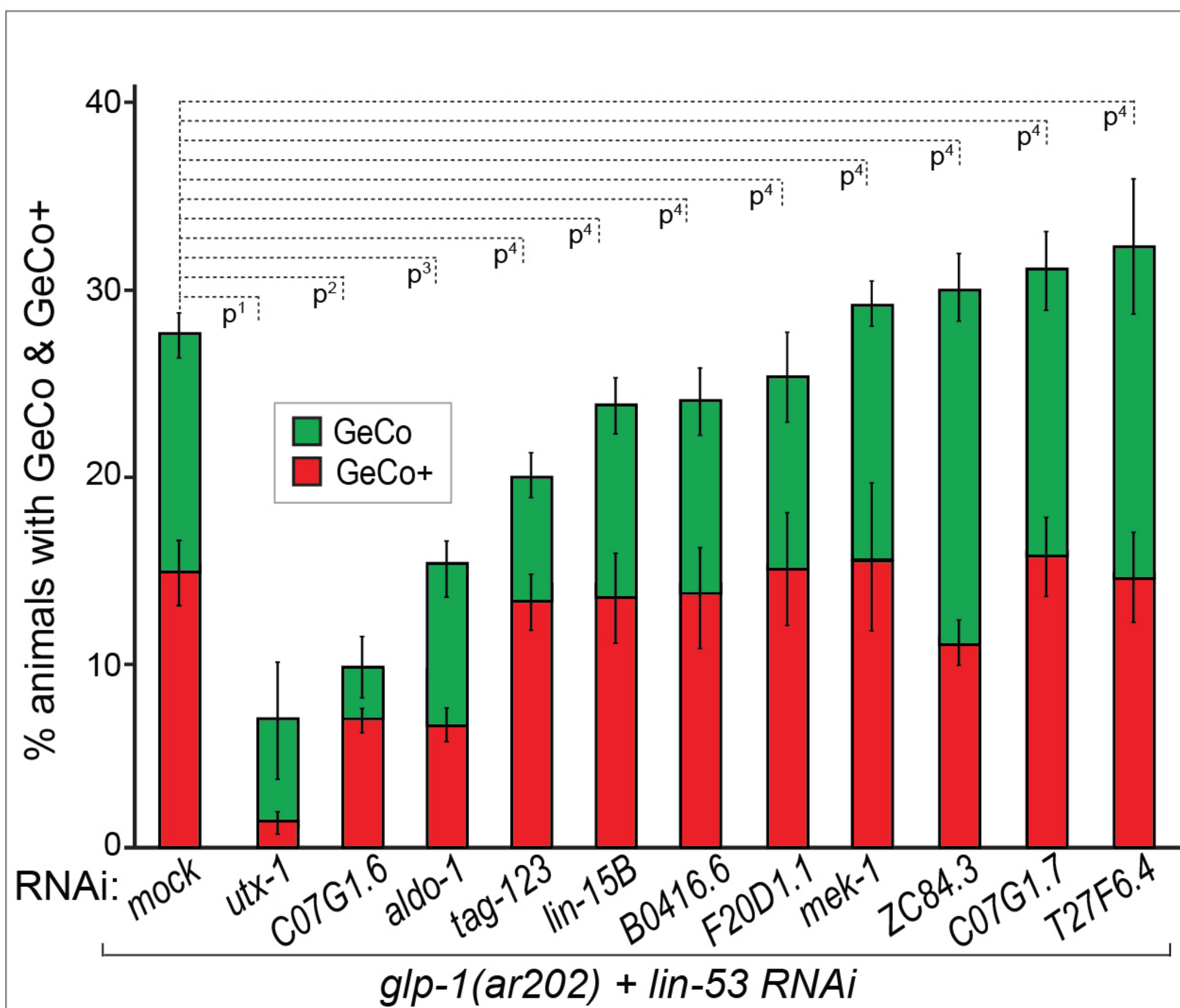




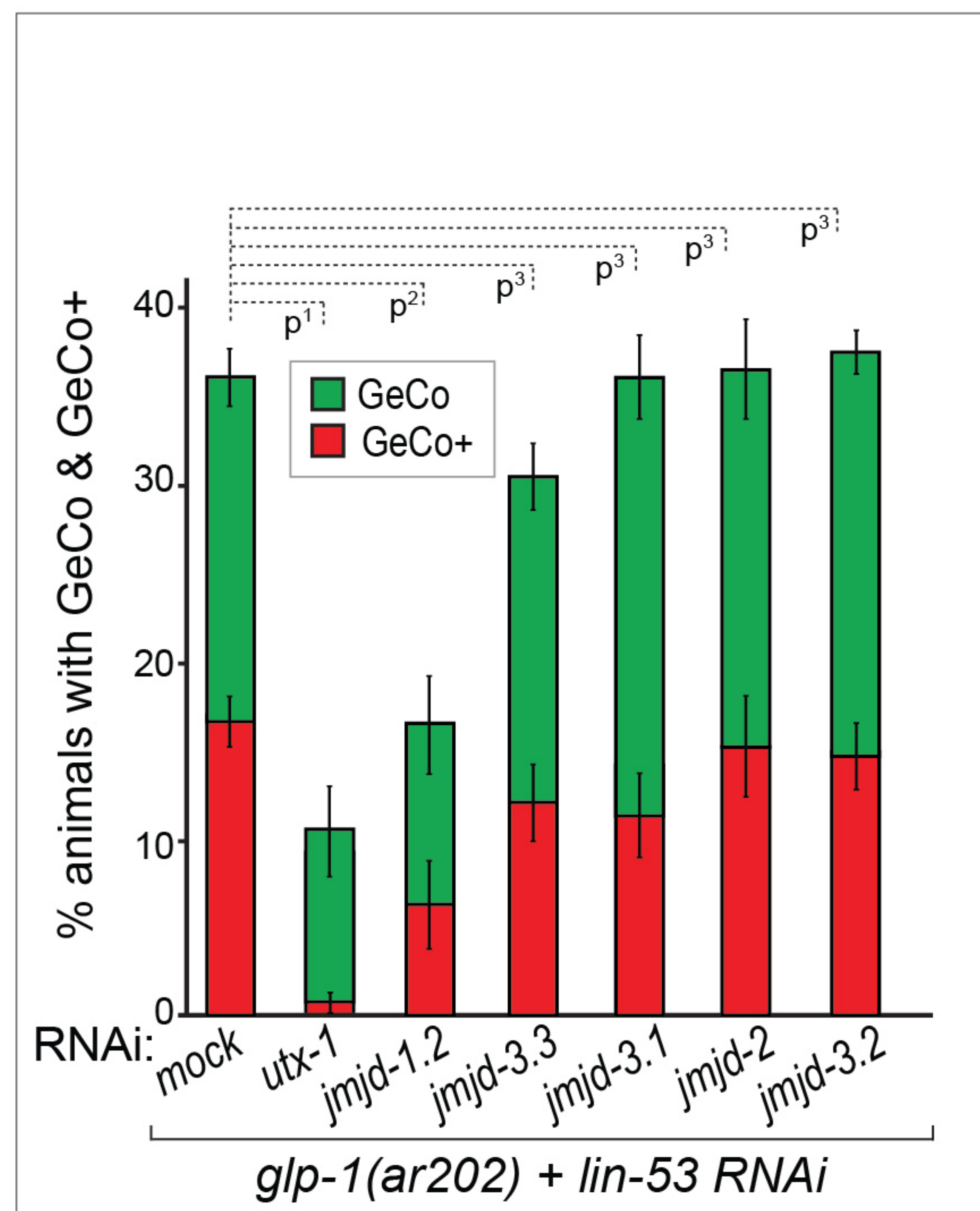




**A**

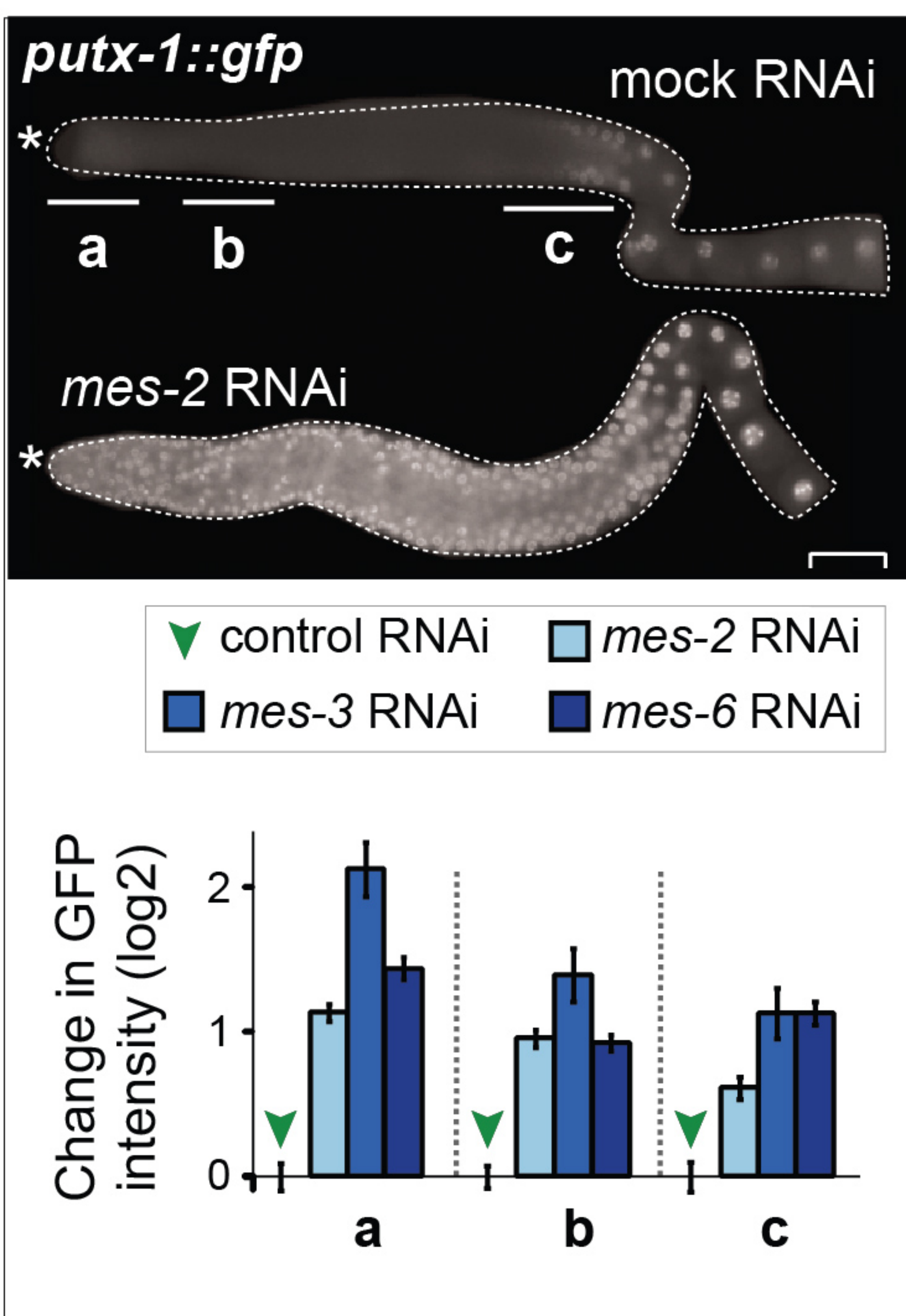


**B**

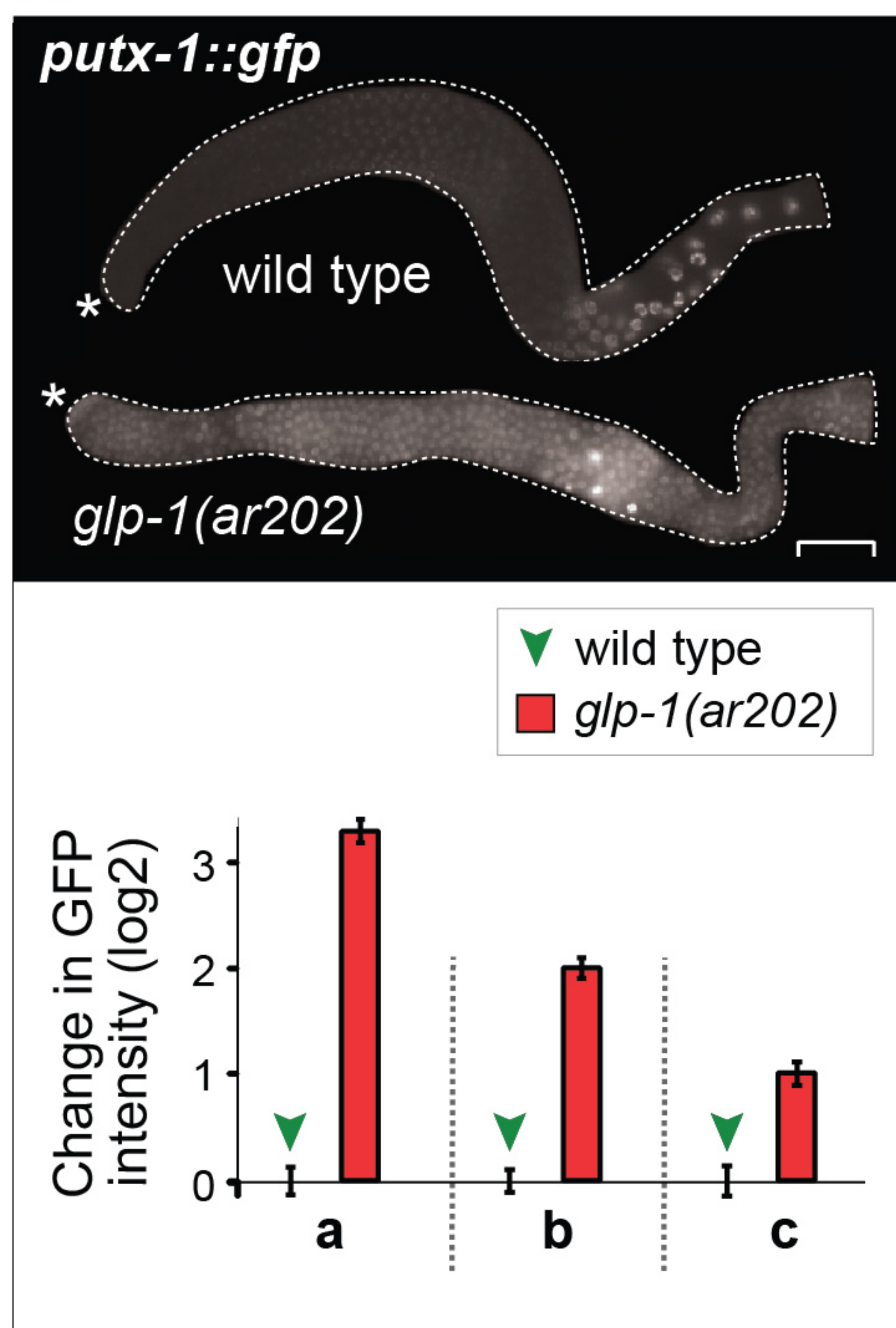




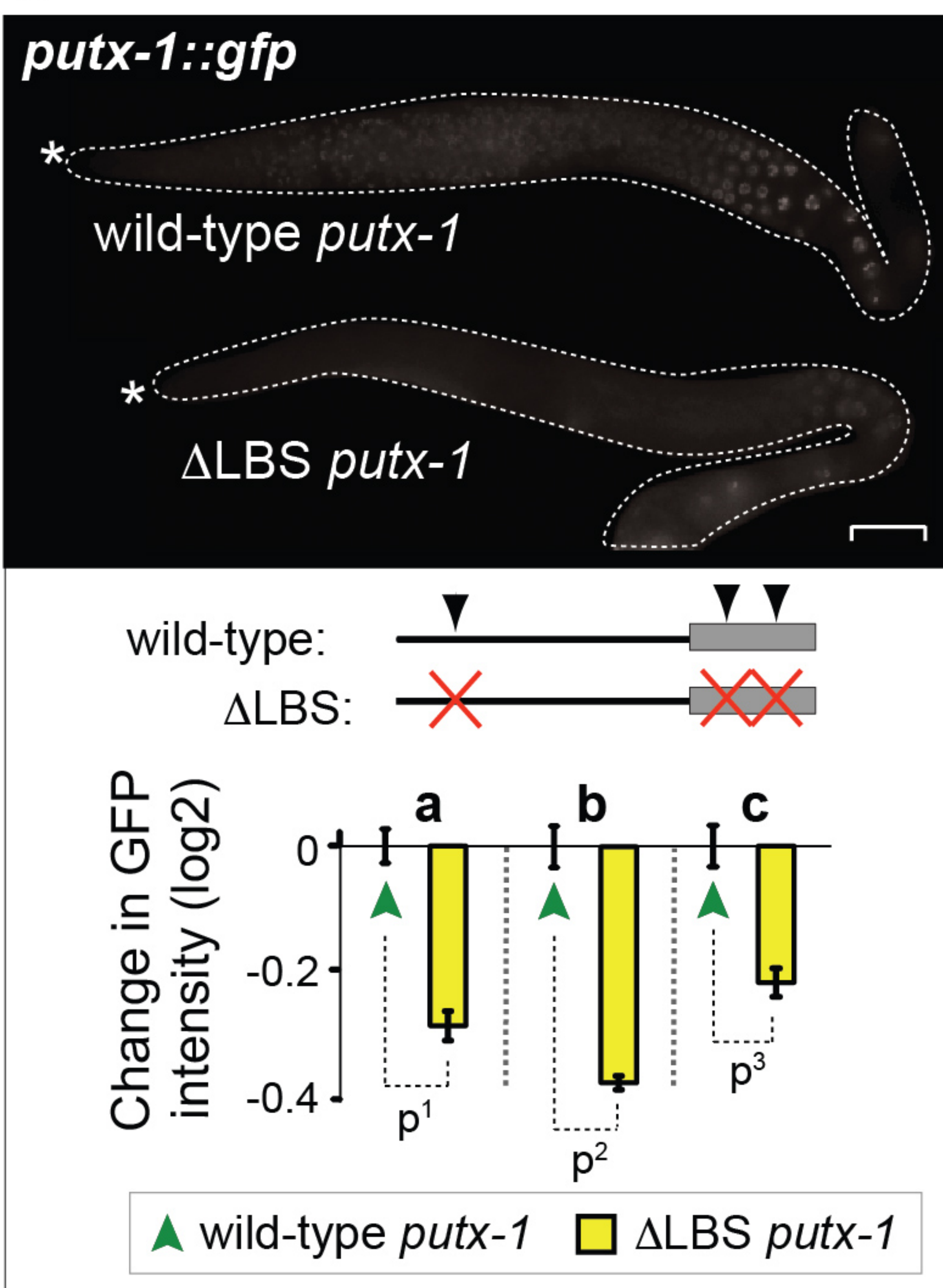
**A**



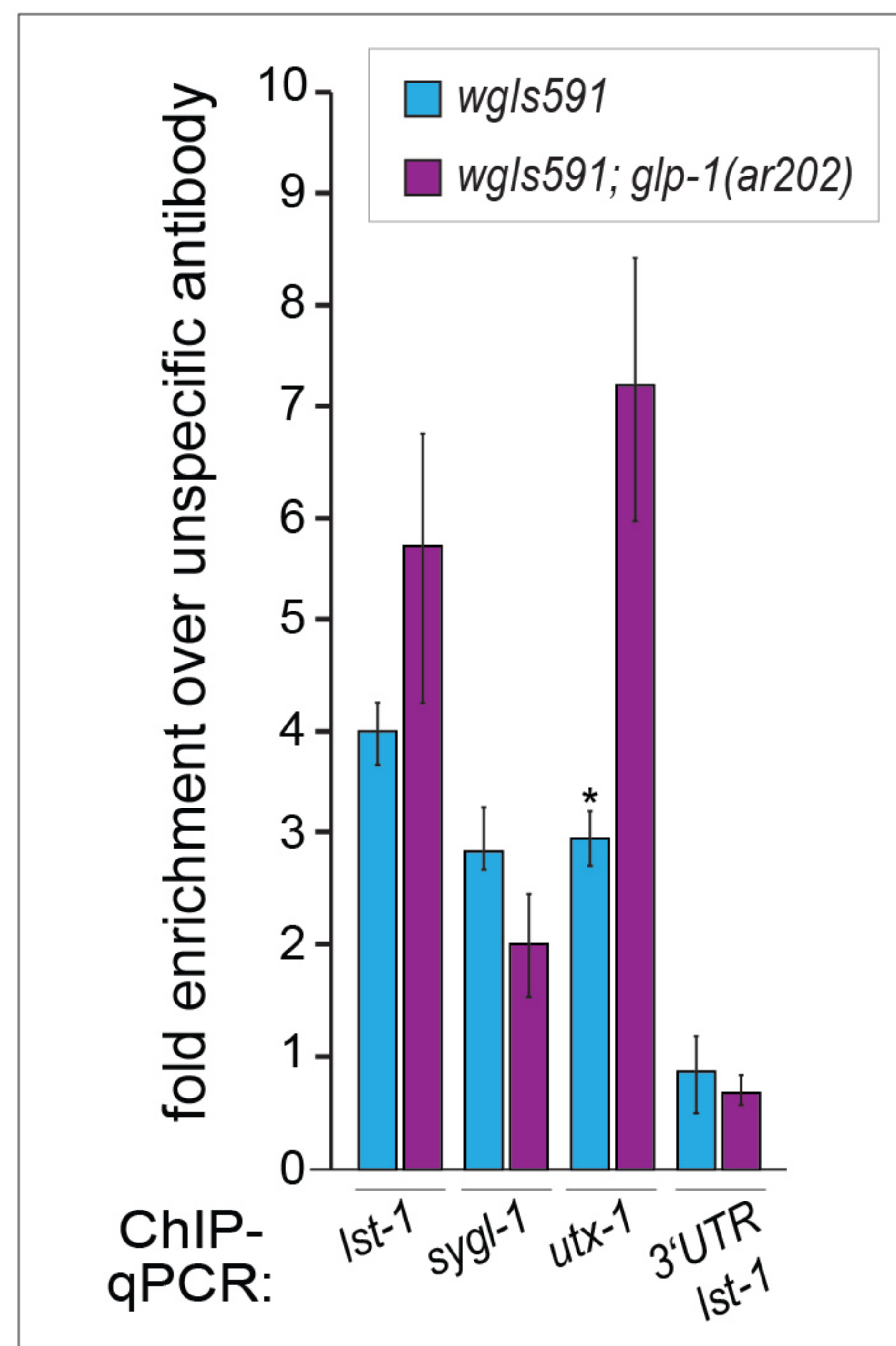
**B**



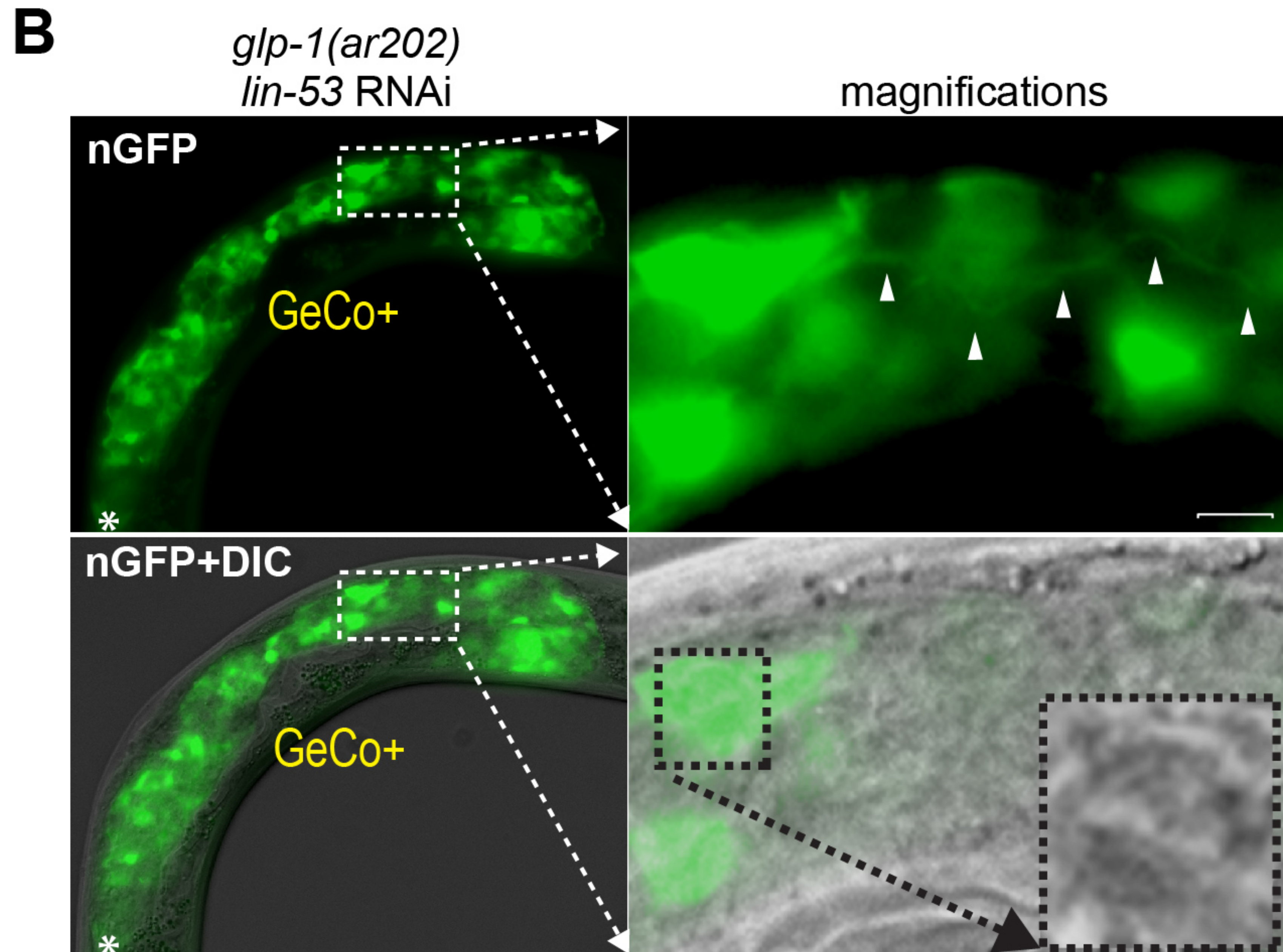
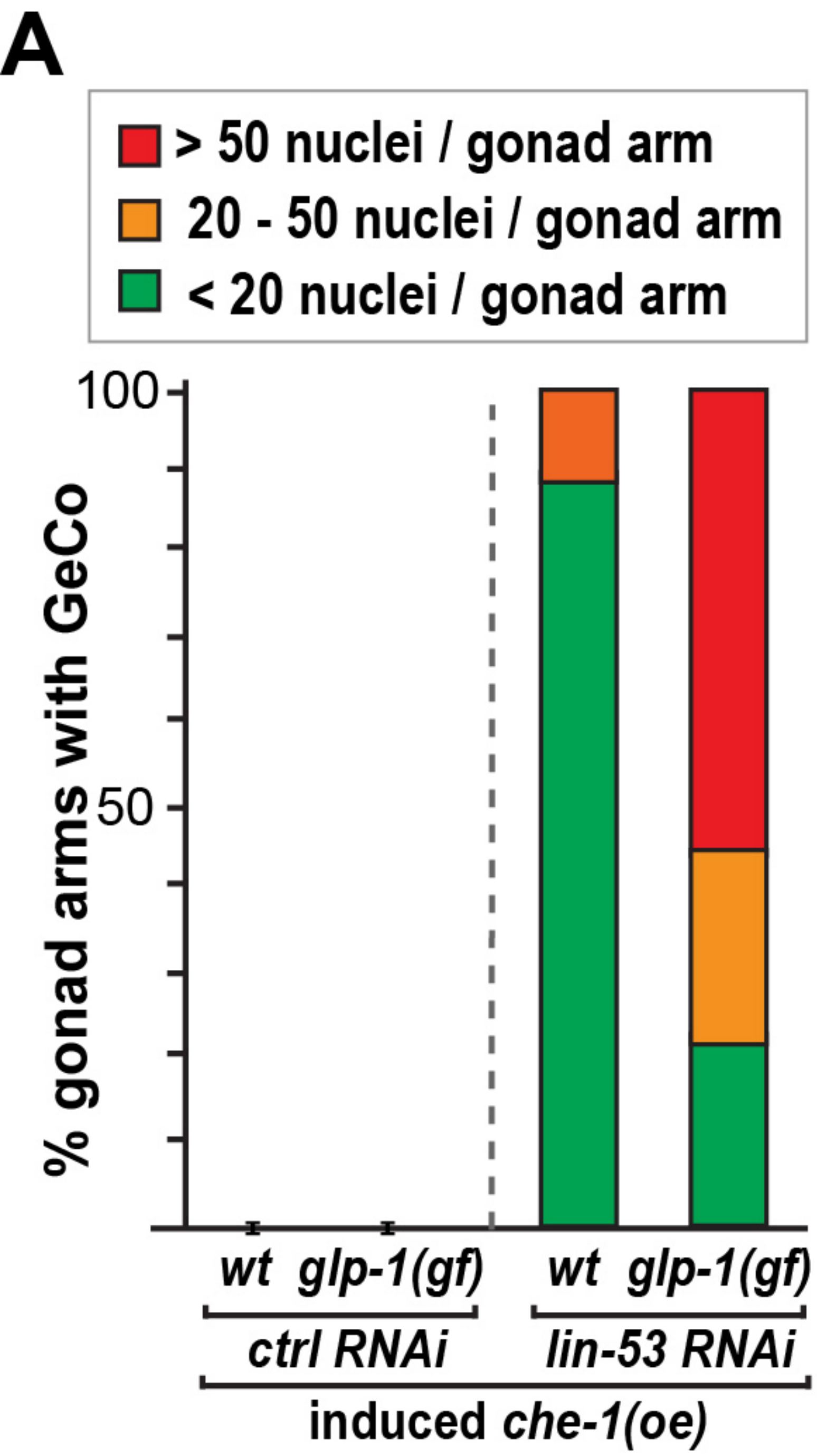
**C**



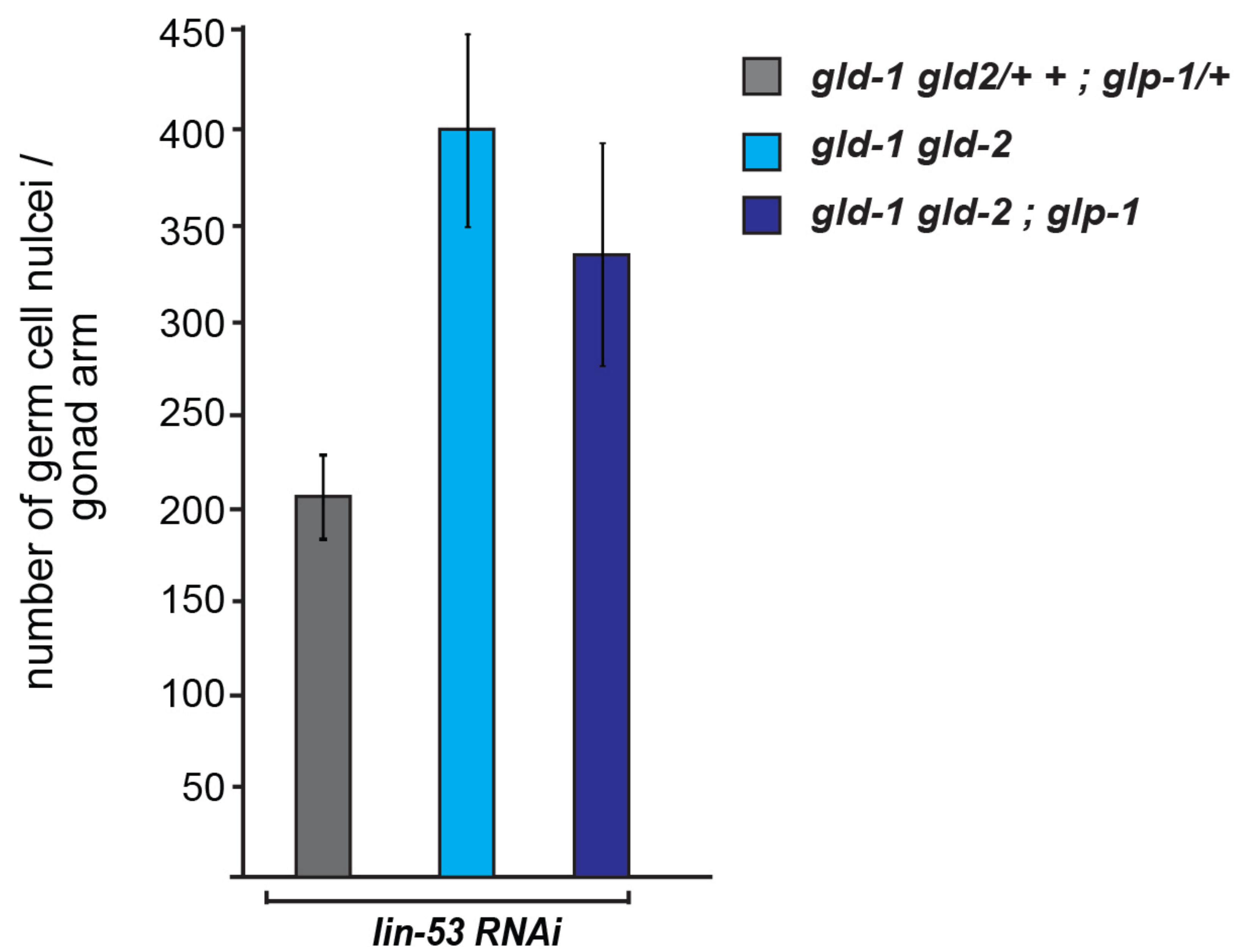
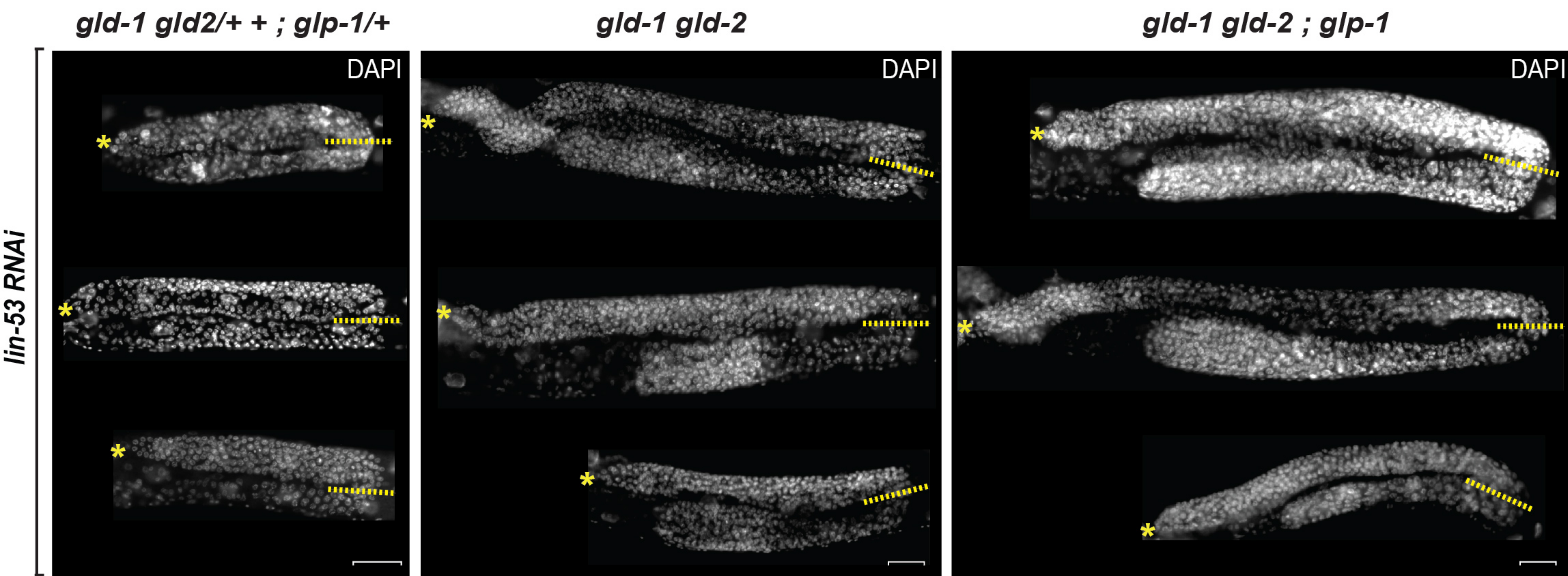
**D**







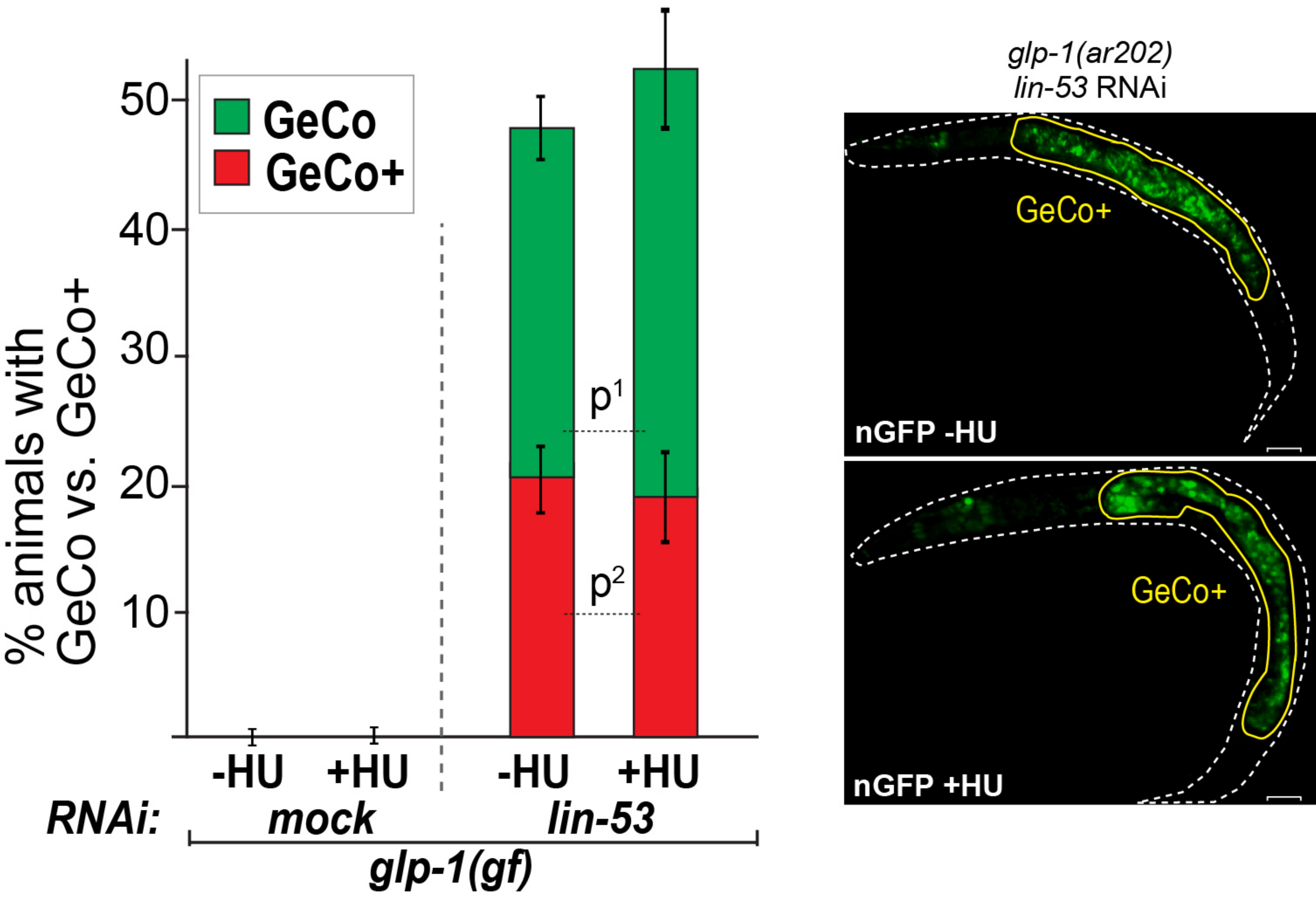




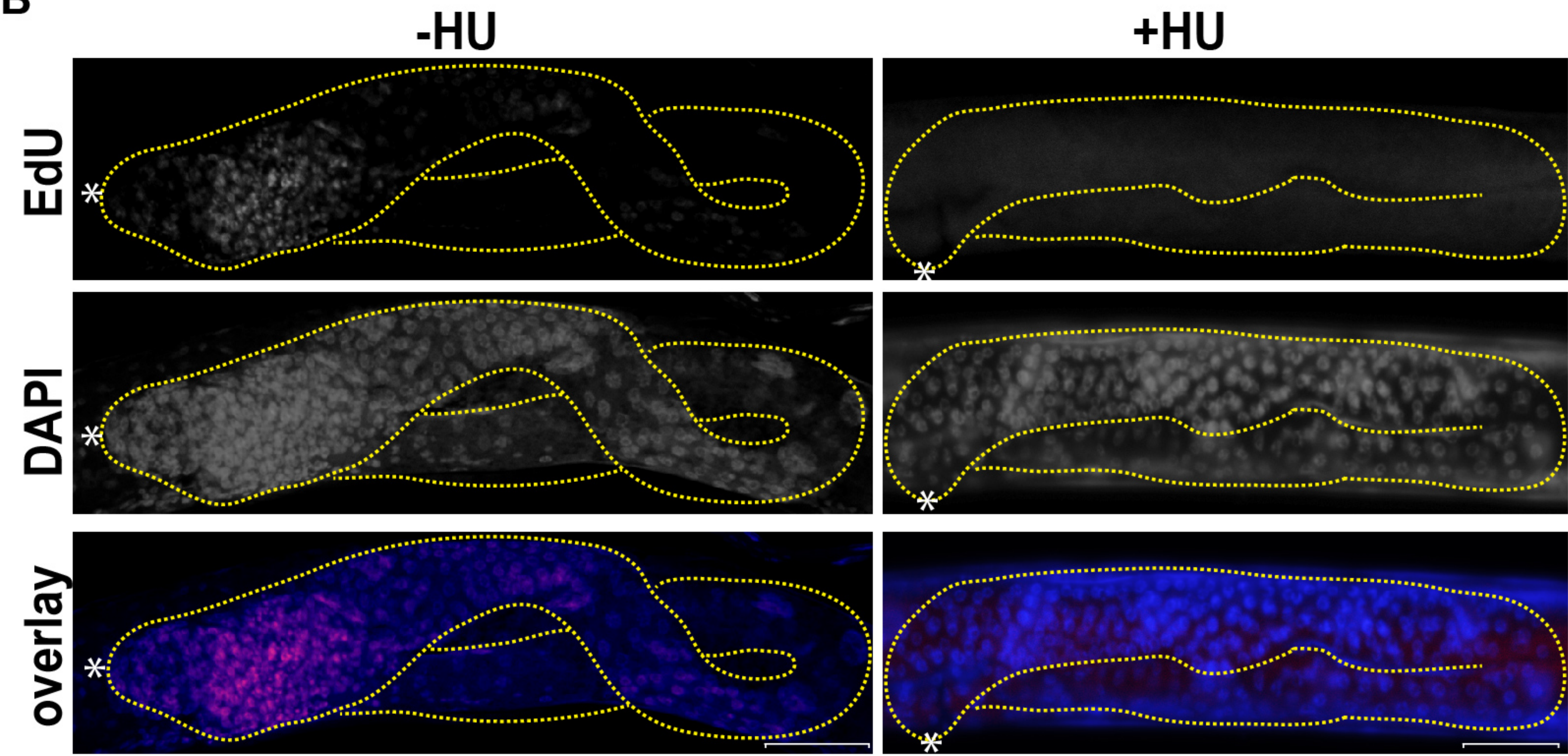


Seelk et al., Figure 1—figure supplement 3

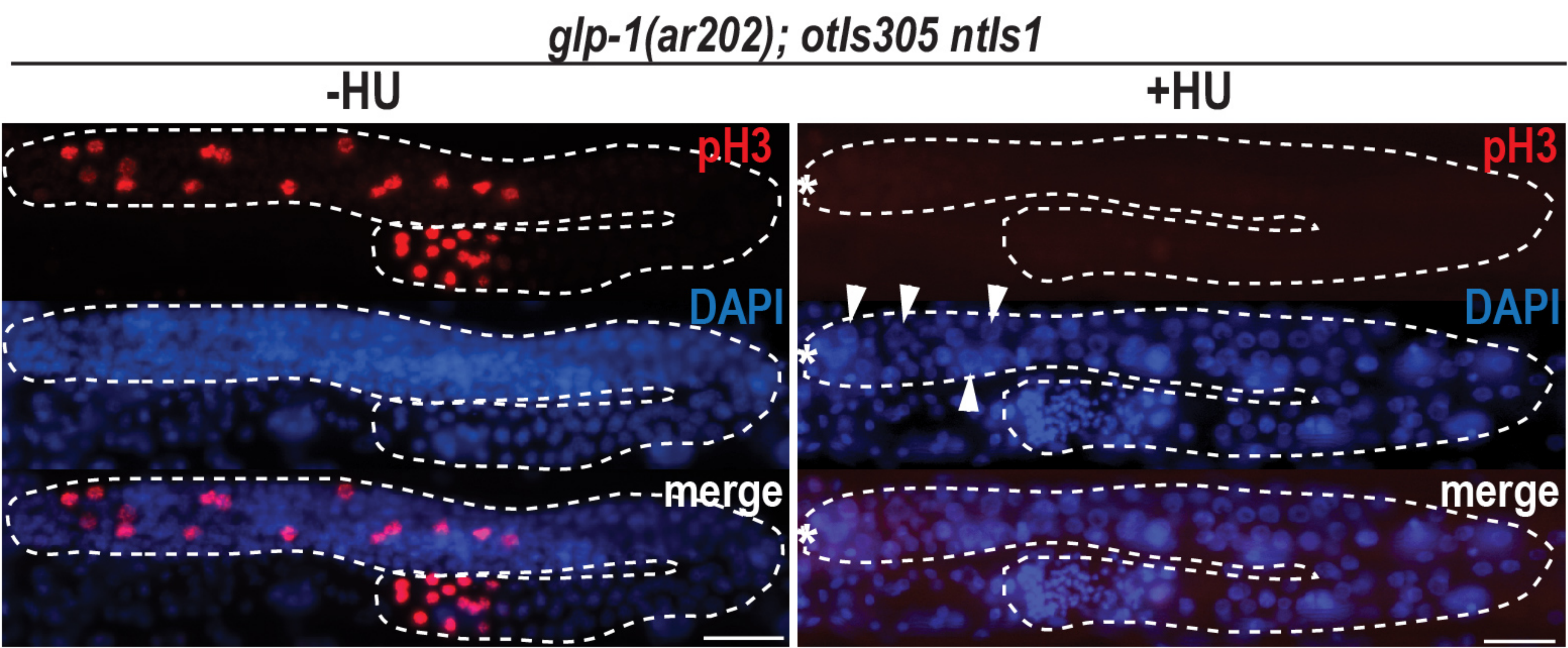
A



B

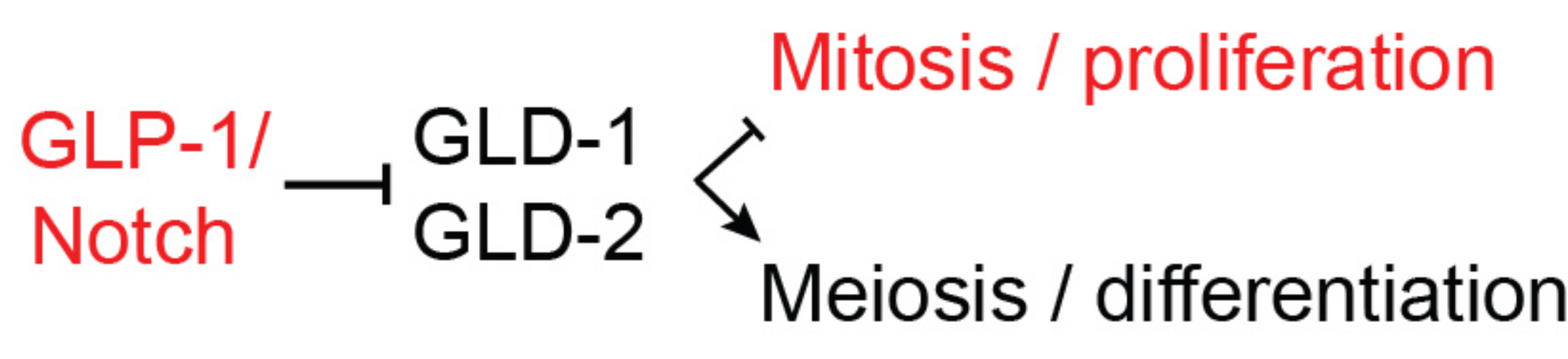


C

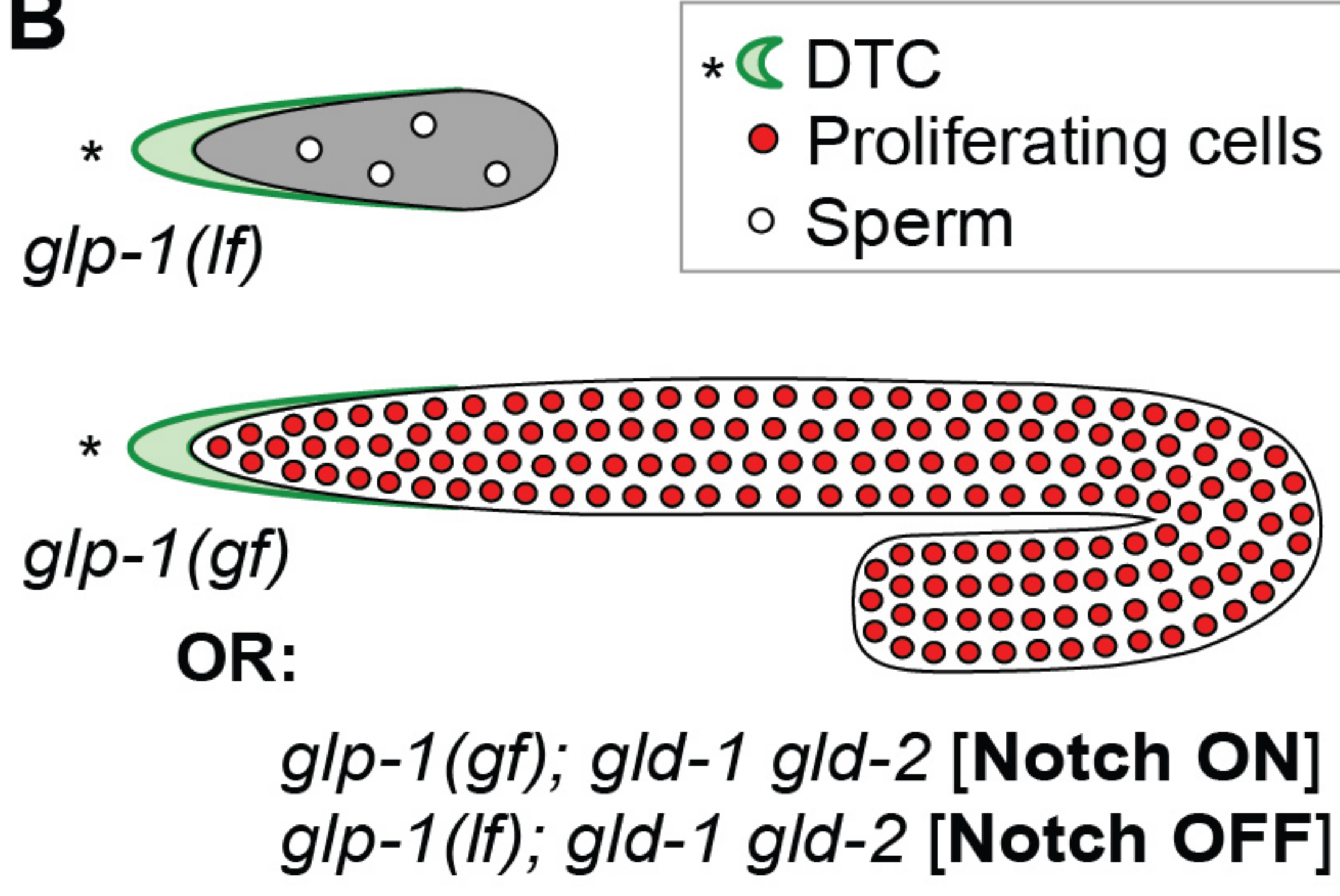




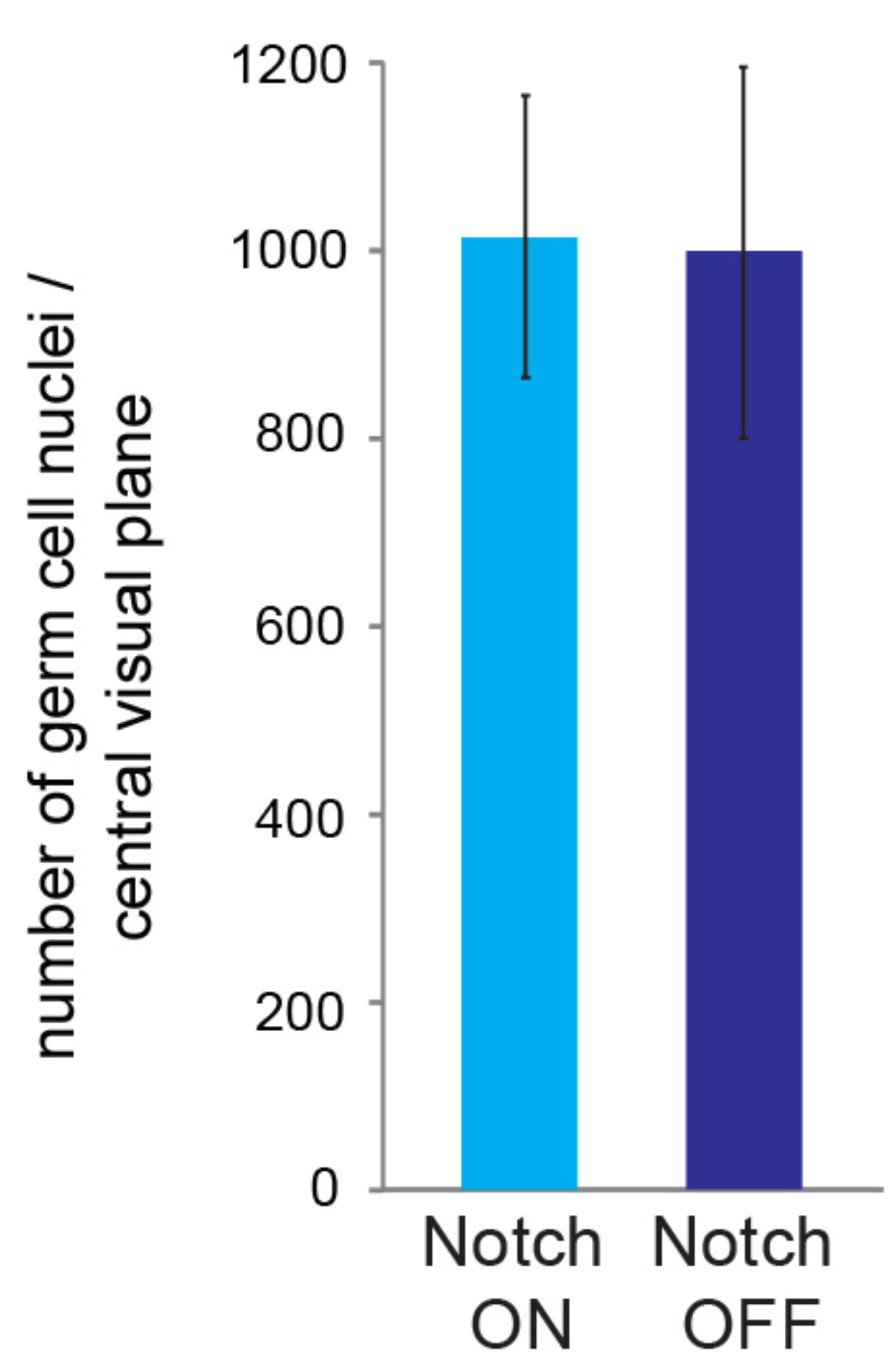
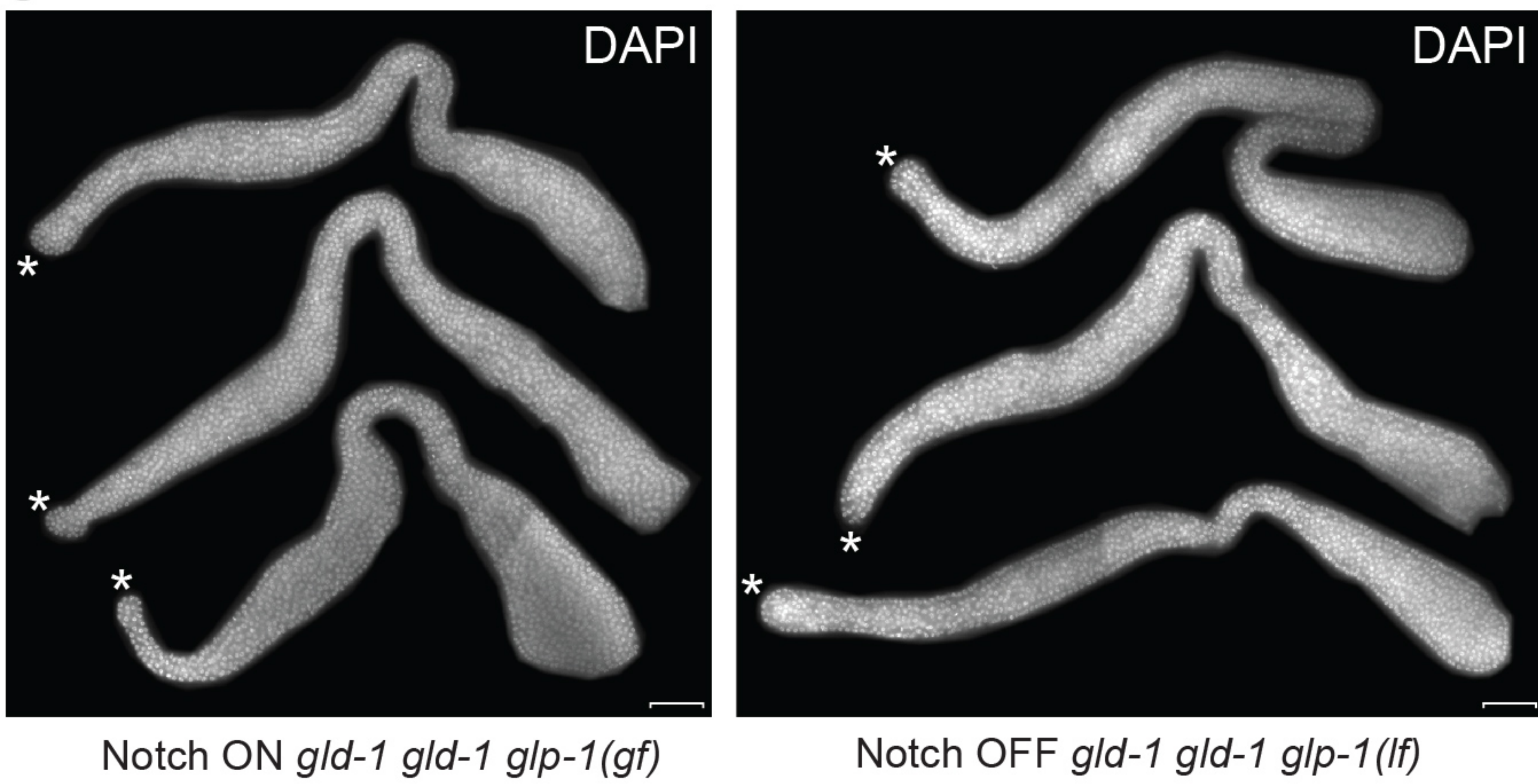
**A**



**B**



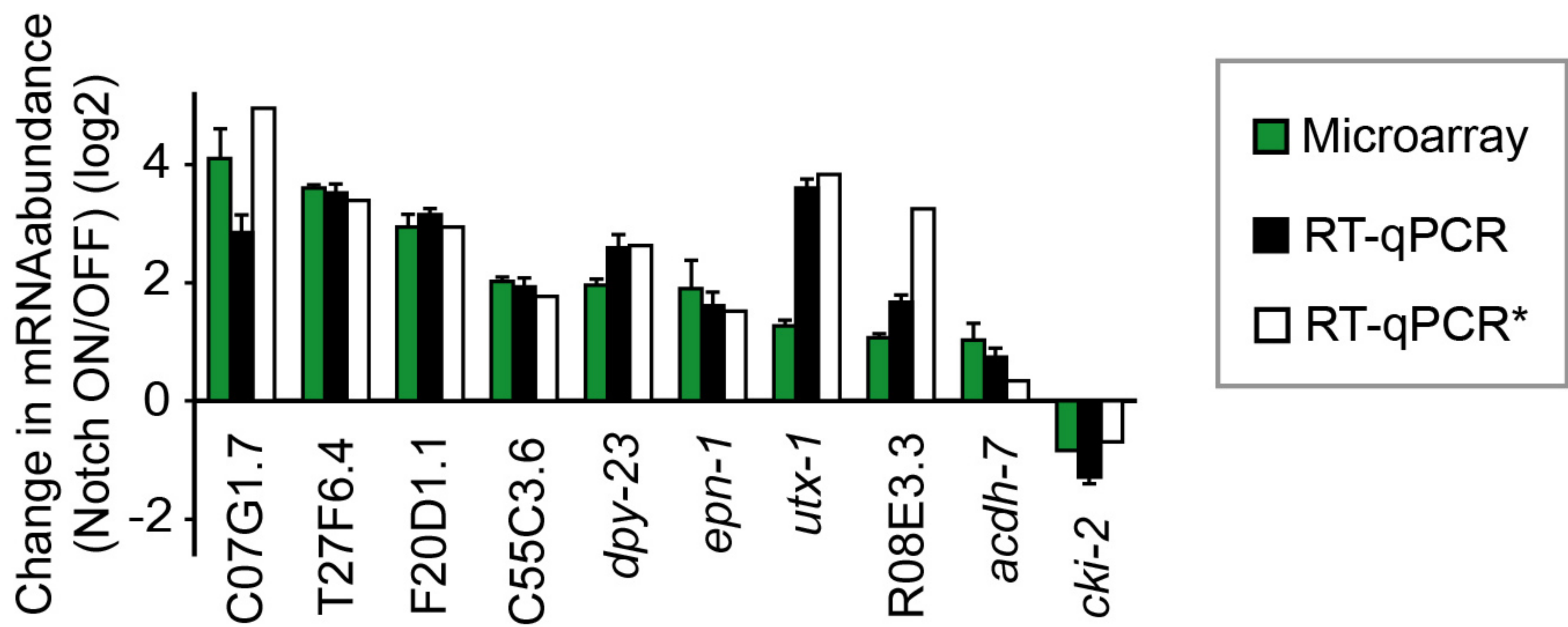
**C**





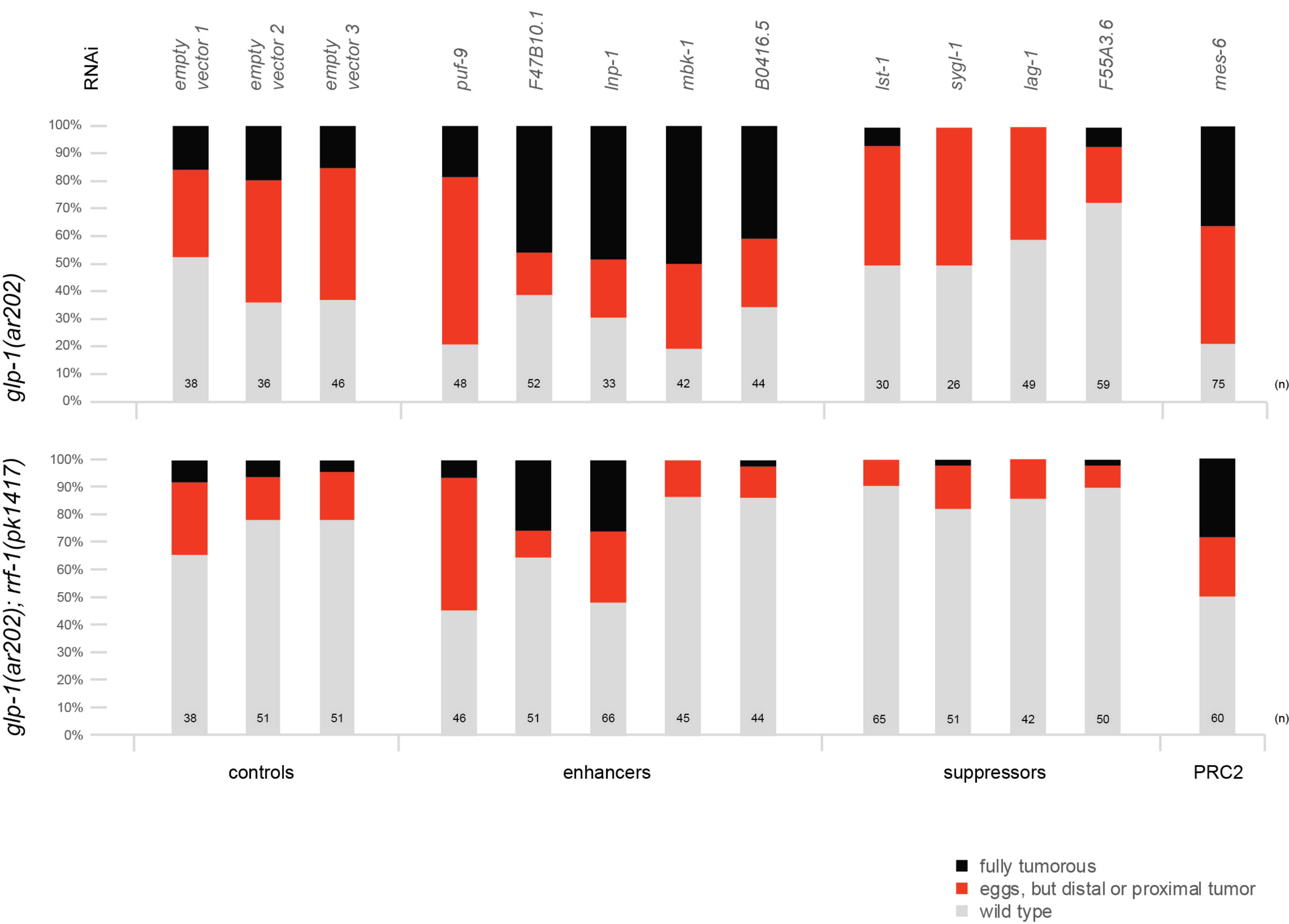
Seelk et al., Figure 2—figure supplement 2

A



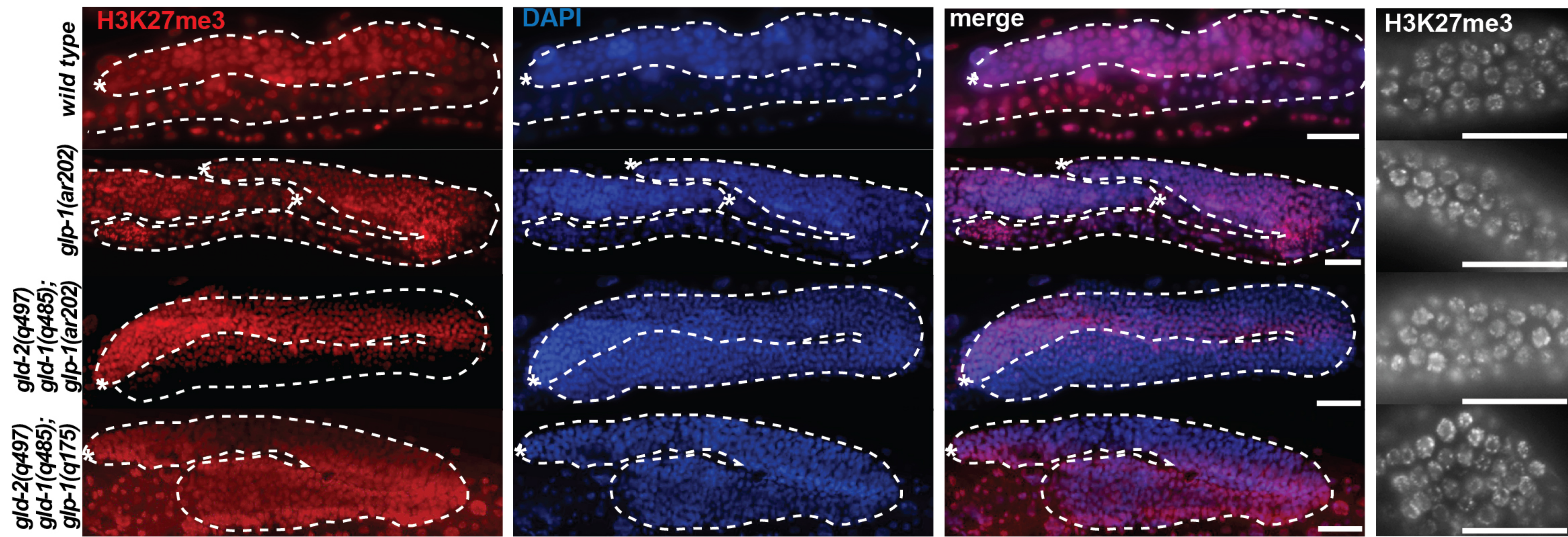
B

Chromosome	All	I.	II.	III.	IV.	V.	X.	Mitochondrial
Total number of genes (%)	17986	2623 (14.58)	3142 (17.47)	2424 (13.48)	2853 (15.86)	4488 (24.95)	2445 (13.59)	11 (0.06)
Total number of GLP-1 Notch activated genes (%)	110	9 (8.18)	10 (9.09)	12 (10.91)	19 (17.27)	10 (9.09)	50 (45.45)	0 (0)
Number of 'expressed' genes (cutoff>=4) (%)	5426	1281 (23.61)	996 (18.36)	1219 (22.47)	964 (17.77)	791 (14.58)	164 (3.02)	11 (0.2)
Number of 'expressed' and GLP-1 Notch activated genes (cutoff>=4) (%)	84	8 (9.53)	7 (8.33)	9 (10.71)	16 (19.05)	5 (5.95)	39 (46.42)	0 (0)



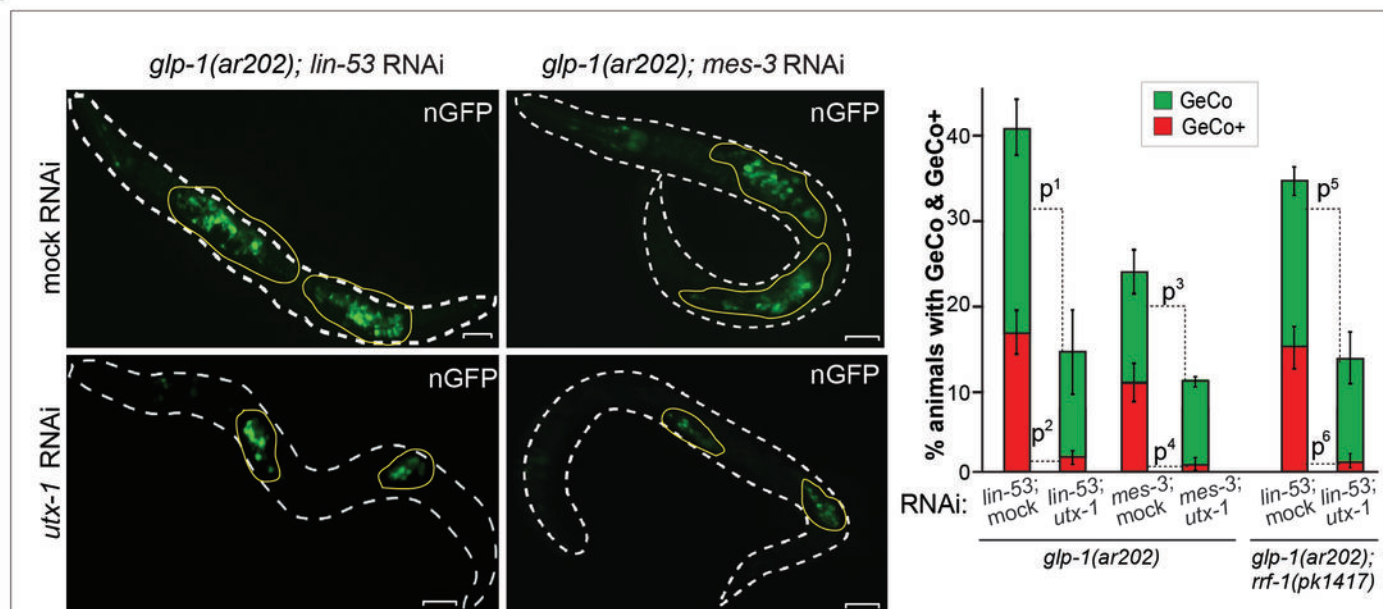


Seelk et al., Figure 2—figure supplement 4

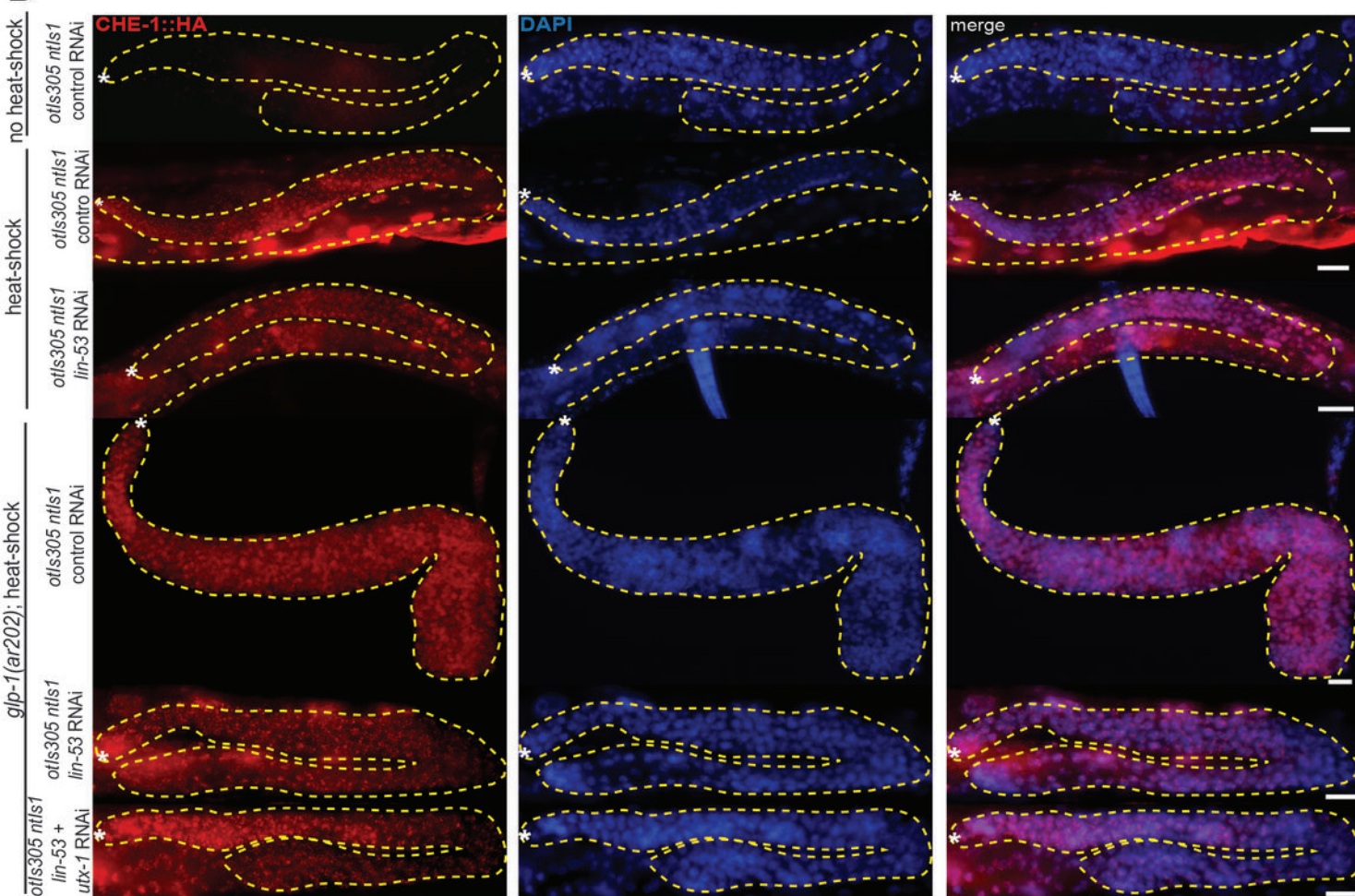




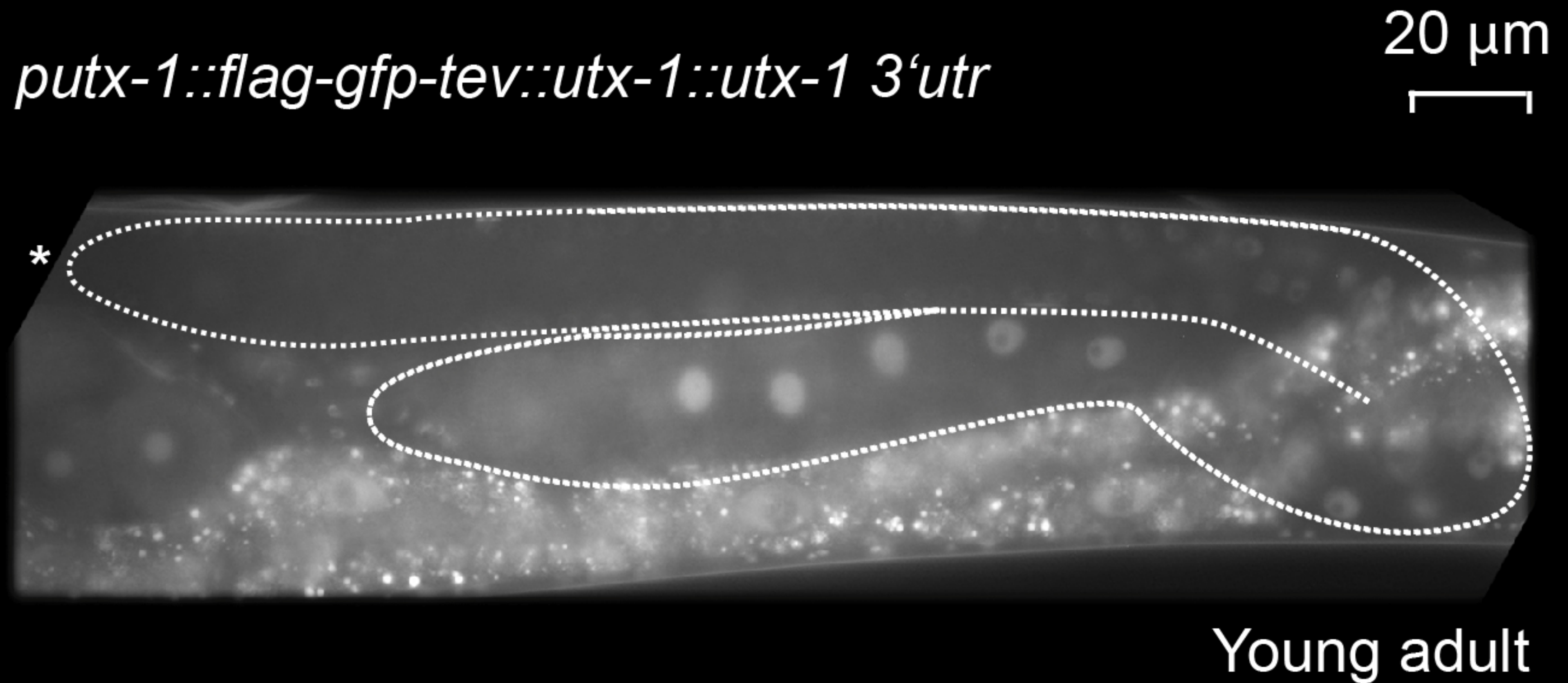
**A**



**B**



# Seelk et al., Figure 5—figure supplement 1





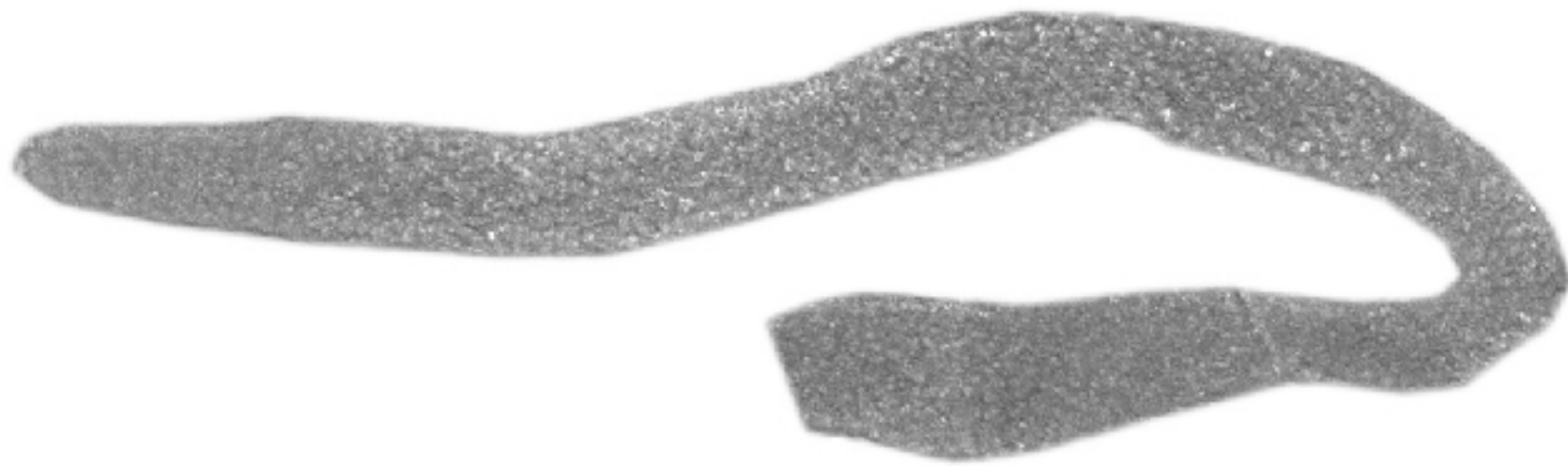
# Seelk et al., Figure 5—figure supplement 2

wild type

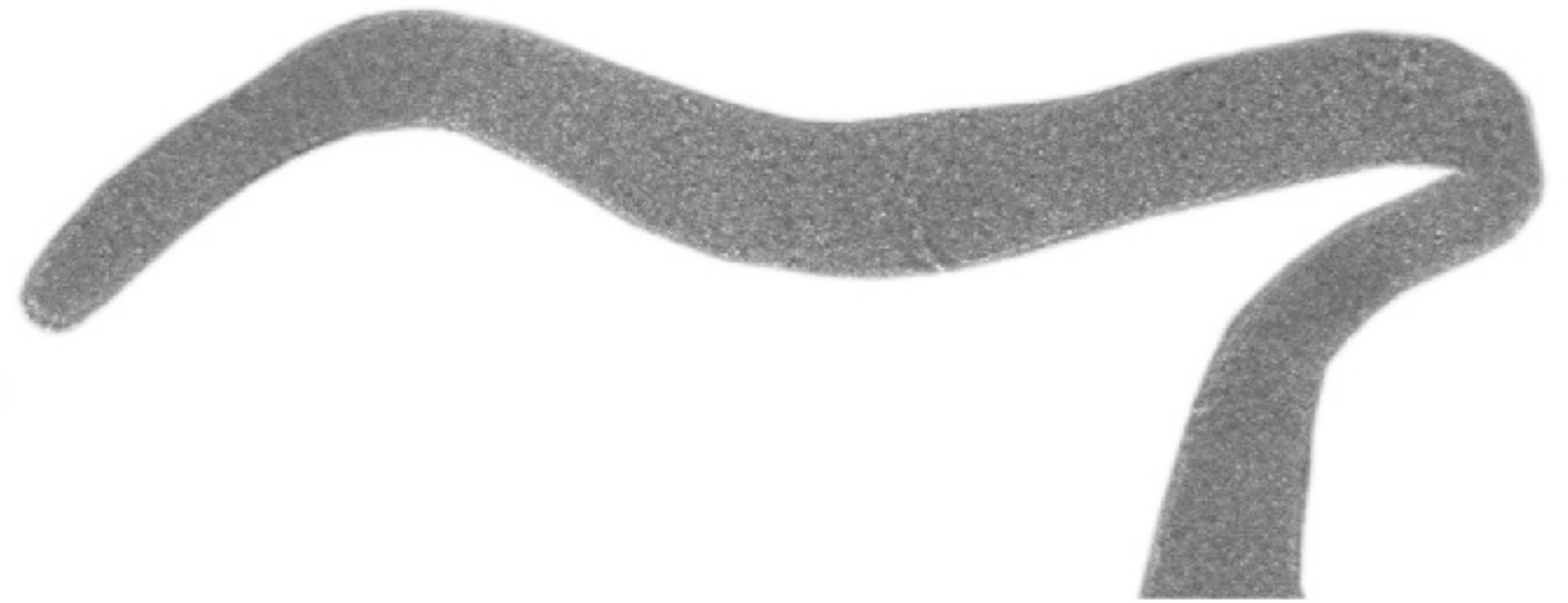
*mes-6*

S

\*



\*



AS

\*



\*



# Seelk et al., Figure 5—figure supplement 3

